Journal Pre-proof

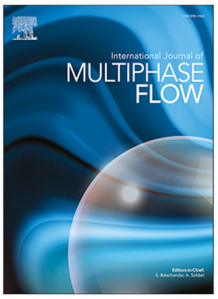

Derivation and stability analysis of two-fluid model equations for bubbly flow with bubble oscillations and thermal damping

Takahiro Ayukai, Tetsuya Kanagawa

PII: S0301-9322(23)00077-0
DOI: https://doi.org/10.1016/j.ijmultiphaseflow.2023.104456
Reference: IJMF 104456

To appear in: *International Journal of Multiphase Flow*

Received date : 3 December 2022
Revised date : 5 March 2023
Accepted date : 22 March 2023

Please cite this article as: T. Ayukai and T. Kanagawa, Derivation and stability analysis of two-fluid model equations for bubbly flow with bubble oscillations and thermal damping. *International Journal of Multiphase Flow* (2023), doi: https://doi.org/10.1016/j.ijmultiphaseflow.2023.104456.

Derivation and stability analysis of two-fluid model equations for bubbly flow with bubble oscillations and thermal damping

Takahiro Ayukai[a], Tetsuya Kanagawa[b]

[a]*Degree Program of Systems and Information Engineering, University of Tsukuba 1-1-1 Tennodai, Tsukuba, 305-0821, Ibaraki, Japan*
[b]*Institute of Systems and Information Engineering, University of Tsukuba 1-1-1 Tennodai, Tsukuba, 305-8573, Ibaraki, Japan*

Abstract

The two-fluid model with bubble oscillations, proposed by Egashira et al. (2004), can explain the properties of cavitating bubbly flow and pressure wave propagation in the bubbly flow. However, the viscous effect as well as energy conservation leading to temperature changes inside the bubble with bubble oscillations have not yet been considered. Therefore, this study aimed to incorporate the viscous (bulk viscosity and drag) and thermal effects to the previously proposed two-fluid model with bubble oscillations. Bulk viscosity was considered by averaging the shear stress term in the single-phase momentum conservation for a Newtonian fluid, and the drag was introduced by transforming the interfacial shear stress. We derived the averaged energy conservation for a general two-phase flow with a thermal conduction inside bubbles and heat transfer between the two phases, and limited this equation to that for a bubbly flow by closing the interfacial temperature gradient term via constitutive equations for a single bubble. Furthermore, we investigated the stability of our proposed one-dimensional model using the linear dispersion analysis. This analysis gave insights as follows: (i) the temperature gradient term in energy conservation can be closed using the temperature gradient models; (ii) the thermal conduction inside bubbles was dominant in the thermal damping rather than the heat transfer between the two phases; (iii) incorporating both the bulk viscosity and drag stabilized our proposed model. Our results is important for developing mathematical models to investigate thermal effects in bubbly flow with bubble oscillations, such as cavitating bubbly flow and wave propagation in bubbly liquids.

Keywords: Bubbly flow, Two-fluid model, Bubble oscillation, Energy conservation, Viscosity, Stability analysis

1. Introduction

Bubbly flow is highly relevant to a variety of phenomena and objects, both natural and synthetic, such as the screws of ships, boiling systems of nuclear power plants, volcanic eruptions, and ultrasound contrast agents. Several researchers have proposed various model equations that simulate the motion of bubbly flow. The one-fluid model, which consists of conservations regarding the two phases as a mixture , is further divided into three models: a homogeneous model, slip flow model, and drift flux model (Kataoka, 2001; Zuber and Findlay, 1965). The two-fluid model, which involves conservation in the gas and liquid phases, has been widely used as it accounts for the relative velocities without restriction of the Stokes number (e.g., Wallis, 1969; Nigmatulin, 1979; Drew, 1983; Prosperetti and Tryggvason, 2007; Ishii and Hibiki, 2010), and and has recently been progressed (Rezende et al., 2015; Vaidheeswaran et al., 2017; de Bertodano et al., 2016; Vaidheeswaran and Lopez de Bertodano, 2016, 2017; Carrillo et al., 2020; Zhang, 2021; Pal and K, 2021; Clausse et al., 2022; Nagrani et al., 2022; Deuben et al., 2022; Shi et al., 2022; Yilgor and Shi, 2022; Habiyaremye et al., 2022).

The majority of bubbly flow models do not consider bubble oscillations owing to an assumption that bubbles behave as solid particles(e.g. Stuhmiller, 1977; Ishii and Hibiki, 2010; Chuang and Hibiki, 2017). In these models, the effects of bubbles on the flow are expressed by the equation derived form the potential flow theory around the particles (e.g. Stuhmiller, 1977; Ishii and Hibiki, 2010; Chuang and Hibiki, 2017). Therefore, properties that consider bubble oscillations are needed. One property is the pressure wave propagation in the bubbly flow, in which the interaction between the pressure wave and bubble oscillations is relatively large. van Wijngaarden (1968, 1972); Prosperetti (1991) incorporated the Rayleigh–Plesset equation into the one-fluid model and derived the Korteweg–de Vrie–Burgers (KdVB) equation that describes a dispersive shock wave in the bubbly flow using the perturbation theory. Our group has derived the KdVB equations from the two-fluid model containing the bubble oscillation model with liquid compressibility (Keller and Kolodner, 1956) under various physical conditions (Kanagawa et al., 2010; Kamei et al., 2021; Yatabe et al., 2021). The other

property considering bubble oscillations in the model is the cavitating bubbly flow. Shock pressure near the bubble surface when the bubble collapses causes cavitation erosion (Rayleigh, 1917). Therefore, incorporating the bubble oscillation model into the two-phase flow model can express the effects of cavitation erosion. Egashira et al. (2004) proposed the two-fluid model with Keller equation (Keller and Kolodner, 1956) that described cavitating bubbly flow by separating the surface-averaged pressure difference at the bubble–liquid interface from the liquid pressure instead of using only the liquid pressure (van Wijngaarden, 1968, 1972; Prosperetti and Jones, 1984). Egashira et al. (2004) stated that identifying the surface and bulk liquid pressures prevented to describe the shock pressure near the bubble surface. This model can be used to calculate the pressure waves in the bubbly flow (Kanagawa et al., 2010; Kamei et al., 2021; Yatabe et al., 2021).

However, the original two-fluid model (Egashira et al., 2004) did not consider the viscous effect, that is, the bulk viscosity and drag. Considering the viscous effect improves the instability of the ill-posed two-fluid model equations (Arai, 1980; Pokharna et al., 1997). Ignoring the viscous effects is one of the reasons for leading to unbounded solutions. The other reasons are, for example, the models of interfacial momentum transfer and the identification of gas and liquid pressure (Stuhmiller, 1977; Lyczkowski et al., 1978; Ramshaw and Trapp, 1978; Lahey et al., 1980; Ransom and Hicks, 1984; Pauchon and Banerjee, 1986; Park et al., 1998; Drew, 1983; Tanamachi and Takahashi, 1995; Yabushita et al., 1995; Lhuillier et al., 2013; Vaidheeswaran and Lopez de Bertodano, 2016, 2017; Tukhvatullina and Frolov, 2018; Panicker et al., 2018; Fox et al., 2020). To provide practical solutions, viscous effect must be considered in the bubbly flow. In addition, the original two-fluid model did not consider temperature changes inside the bubbles. Strong bubble oscillations can increase the temperature inside the bubbles in cavitation flow. The temperature change inside the bubbles cannot also be neglected for the pressure waves in the bubbly flow. Prosperetti (1991) are the pioneers who studied the bubbly flow model with bubble oscillations by incorporating the thermal effects. They theoretically and numerically investigated pressure wave propagation with thermal effects by incorporating the differential equation for the gas pressure of a single bubble (see Eq. (41)) and the energy conservation inside a single bubble (Prosperetti et al., 1988) into the simplified one-fluid model (Caflisch et al., 1985) and showed that the thermal effect caused the attenuation of the pressure wave. Furthermore, Fuster and Montel (2015) theoretically investigated the pressure wave attenuation

in bubbly liquids by incorporating both the thermal and mass-transfer effects into the one-fluid model. Although the two-fluid model by Egashira et al. (2004) can express the high pressure at the interface in the cavitation flow, energy conservation of the two-fluid model with bubble oscillations, which can describe the temperature change, has not yet been clearly elucidated.

Therefore, this study aimed to incorporate the viscous effects into the momentum conservations of the original two-fluid model and derive energy conservation to consider the temperature change inside bubbles with oscillations. The two-fluid model primarily uses one of the three averaging processes: time averaging (e.g. Ishii, 1975; Drew, 1983; Ishii and Hibiki, 2010), volume averaging (e.g. van Deemter and van der Laan, 1961; Nigmatulin, 1979; Prosperetti and Jones, 1984), and ensemble averaging (e.g. Drew, 1983; Joseph et al., 1990; Zhang and Prosperetti, 1994; Drew and Passman, 1998). Through these methods, the quantities can be averaged over a relatively long time, large control volume containing several bubbles, and large number of realisations, respectively. In this study, we used a volume averaging to analytically transform interfacial terms in the momentum and energy conservations.

The reminder of the paper is organised as follows: the volume-averaging technique and the process of deriving the averaged momentum conservation are described in Sections 2.1 and 2.2. We incorporated the bulk viscosity and drag into the averaged momentum conservations, described in Section 2.3. Instead of introducing only the differential equation for the gas pressure (Prosperetti et al., 1988; Prosperetti, 1991), we derived the volume-averaged energy equation from the energy balance in the control volume and closed the interfacial gradient term using equations for a single bubble. We used the following assumptions for deriving averaged momentum conservations: (i) bubbles do not coalesce, break up, become extinct, and appear; (ii) the bubble–bubble interaction is ignored; (iii) the gas pressure inside bubbles is uniform in the control volume; (iv) the bubble radius is uniform the control volume; (v) the liquid phase is isothermal; (vi) the gas inside the bubbles is an ideal gas; (vii) the effect of mass transfer is neglected. (i) and (vii) are valid when the phase change between the gas and liquid is negligible. The effect of the phase change on the bubbly flow modeling with bubble oscillations was discussed by Fuster and Montel (2015). (ii)–(iv) are valid when a control volume is sufficiently smaller than a scale of macroscopic flows and larger than a scale of bubbles. Hence, our presented two-fluid model equations can cover that a void fraction α is relatively small ($\alpha \lesssim 0.01$) and an appropriate grid scale is considered in numerical situations. Although (v)

and (vi) are considered to simplify the derivation of the energy conservation, these assumptions are valid when the gas inside bubbles is air and α is relatively small. Finally, we discussed the stability of the proposed two-fluid model equations with bubble oscillations using the linear dispersion analysis in Section 3.

2. Two-fluid model equations with bubble oscillations

This section provides a detailed description of deriving the two-fluid model equations with bubble oscillations. The first step introduces the volume-averaging process, and then the volume-averaged momentum and energy conservations are derived. The important point of deriving is the transforming method of interfacial terms in both conservations.

2.1. Volume-averaging process

In this section, we introduce three types of volume-averaging techniques (e.g. Drew, 1983; Prosperetti and Jones, 1984; Egashira et al., 2004) to describe the short time scale of bubble oscillations. First, the space average for a variable $\phi(\boldsymbol{y}, t)$ was defined at a given $\boldsymbol{x}$ as,

$$\langle\phi\rangle(\boldsymbol{x}, t) = \frac{1}{V}\int_{\Omega} g(\boldsymbol{y}-\boldsymbol{x})\phi(\boldsymbol{y}, t)\mathrm{d}V(\boldsymbol{y}), \tag{1}$$

where $\boldsymbol{y}$ is the local position, V is the control volume, $\boldsymbol{x}$ is the center position of the control volume, Ω is a sufficiently large volume containing V, and $g(\boldsymbol{y}-\boldsymbol{x})$ is a discontinuous function, which returns 1 for $|\boldsymbol{y}-\boldsymbol{x}| \leq$ radius of V and 0 for others . Second, the space average for a variable $\phi(\boldsymbol{y}, t)$ in the k-th phase was defined at a given $\boldsymbol{x}$ as,

$$\overline{\phi_k}(\boldsymbol{x}, t) = \frac{1}{V_k(\boldsymbol{x}, t)}\int_{\Omega} g(\boldsymbol{y}-\boldsymbol{x})X_k(\boldsymbol{y}, t)\phi(\boldsymbol{y}, t)\mathrm{d}V(\boldsymbol{y}), \tag{2}$$

where V_k is the volume occupied by phase k in V and $X_k(\boldsymbol{y}, t)$ is the phase indicator function, which is defined as,

$$X_k(\boldsymbol{y}, t) = \begin{cases} 1, & \text{if } \boldsymbol{y} \text{ is in } V_k, \\ 0, & \text{otherwise}, \end{cases} \tag{3}$$

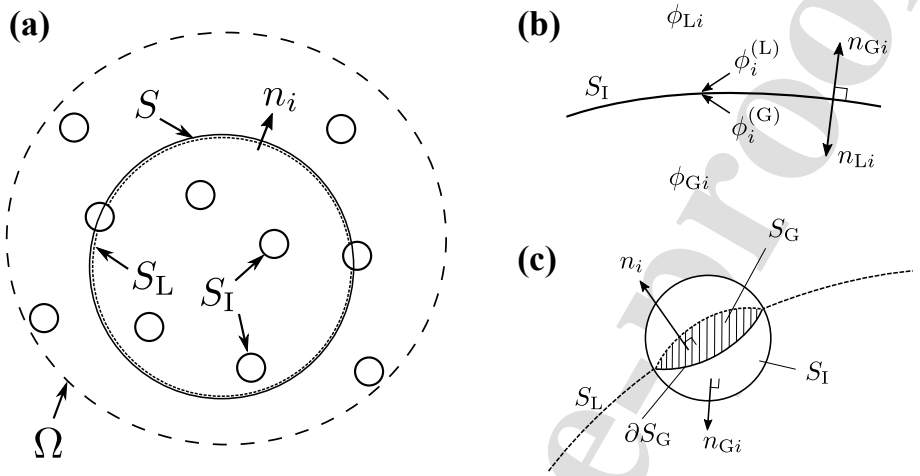

Figure 1: (a) Control volume V in a mixture of liquid and spherical gas bubbles Ω: S is the surface of V; S_{L} is the liquid component of S, S_{G} is the gaseous component of S, S_{I} is the surface of bubbles in V, and n_i is the normal vector at S. (b) Enlarged view of S_{I}: $n_{\mathrm{G}i}$ is the normal vector toward the outside of the bubbles, $n_{\mathrm{L}i}$ is the normal vector toward the insides of the bubbles, and superscript (k) signifies the quantity of k-th phase at the interface S_{I}. (c) Bubble cutting by the control volume V: ∂S_{G} is the boundary of S_{G}.

where $k = \mathrm{L}$ denotes the liquid phase and $k = \mathrm{G}$ denotes the gas phase. Third, a mass-weighted phase average for variable $\phi(\boldsymbol{y}, t)$ was defined at a given $\boldsymbol{x}$ as,

$$\widehat{\phi_k}(\boldsymbol{x}, t) = \frac{1}{\overline{\rho_k}(\boldsymbol{x}, t) V_k(\boldsymbol{x}, t)} \int_\Omega g(\boldsymbol{y} - \boldsymbol{x}) X_k(\boldsymbol{y}, t) \rho(\boldsymbol{y}, t) \phi(\boldsymbol{y}, t) \mathrm{d}V(\boldsymbol{y}), \tag{4}$$

where ρ is the density.

2.2. Mass conservations

A volume-averaged conservation equation can be derived via the application of Eqs. (1)–(4) to a single-phase conservation equation (Drew, 1983; Egashira et al., 2004). The mass conservation equation in the k-th phase becomes

$$\frac{\partial}{\partial t}(\alpha_k \overline{\rho_k}) + \frac{\partial}{\partial x_i}(\alpha_k \overline{\rho_k} \widehat{u_{ki}}) = \left\langle \rho(u_i - u_i^\dagger) \frac{\partial X_k}{\partial y_i} \right\rangle, \tag{5}$$

where t is the time, α_k is the volume fraction of the k-th phase, u_i is the velocity, and $u_i^\dagger$ is the velocity of the gas–liquid interface. In this study, $u_i - u_i^\dagger$ is zero because phase changes were not considered. Hence, the volume-averaged mass conservations in the gas and liquid are given as,

$$\frac{\partial}{\partial t}(\alpha_{\mathrm{G}}\overline{\rho_{\mathrm{G}}}) + \frac{\partial}{\partial x_i}(\alpha_{\mathrm{G}}\overline{\rho_{\mathrm{G}}}\widehat{u_{\mathrm{G}i}}) = 0, \tag{6}$$

$$\frac{\partial}{\partial t}(\alpha_{\mathrm{L}}\overline{\rho_{\mathrm{L}}}) + \frac{\partial}{\partial x_i}(\alpha_{\mathrm{L}}\overline{\rho_{\mathrm{L}}}\widehat{u_{\mathrm{L}i}}) = 0. \tag{7}$$

2.3. Momentum conservations

As well as the averaged mass conservations, the averaged momentum conservation can be derived via the application of Eqs. (1)–(4) to a single-phase conservation equation (Drew, 1983; Egashira et al., 2004) as

$$\begin{aligned}
&\frac{\partial}{\partial t}(\alpha_k\overline{\rho_k}\widehat{u_{ki}}) + \frac{\partial}{\partial x_j}(\alpha_k\overline{\rho_k}\widehat{u_{ki}}\widehat{u_{kj}}) \\
&= -\frac{\partial}{\partial x_i}(\alpha_k\overline{p_k}) + \frac{\partial}{\partial x_j}\left[\alpha_k\overline{\mu_k\left(\frac{\partial u_{ki}}{\partial y_j} + \frac{\partial u_{kj}}{\partial y_i}\right)}\right] - \frac{\partial}{\partial x_j}\left(\alpha_k\overline{\rho_k}\widehat{u'_{ki}u'_{kj}}\right) \\
&\quad - \frac{1}{V}\int_{\mathrm{S_I}} p^{(k)} n_{ki}\mathrm{d}S + \frac{1}{V}\int_{\mathrm{S_I}}\left[\mu\left(\frac{\partial u_j}{\partial y_i} + \frac{\partial u_i}{\partial y_j}\right)\right]^{(k)} n_{kj}\mathrm{d}S,
\end{aligned} \tag{8}$$

where p is the pressure, μ is the viscosity, and u'_i is the fluctuation of the mass-weighted phase-averaged velocity. The third term on the right-hand side of Eq. (8) represents the Reynolds stress in the k-th phase. This term can be modelled, for example, using the Reynolds-Averaged Navier–Stokes (Sato and Sekoguchi, 1975; Lee et al., 2017; Lubchenko et al., 2018); however, it is not considered in the present study. The last two terms on the right-hand side of Eq. (8) are expressed in terms of integrals of non-averaged quantities, where $\mathrm{S_I}$ is the total gas–liquid interface in V, n_{kj} is the unit normal vector at the interface $\mathrm{S_I}$, and the value with superscript (k) signifies the quantity of the k-th phase at the interface (Fig. 1 (a) and (b)). These two terms represent the gas–liquid interfacial phenomena, which were derived using the following relation (Prosperetti and Jones, 1984; Egashira et al., 2004):

$$\left\langle \phi_j(\boldsymbol{y},t)\frac{\partial X_k(\boldsymbol{y},t)}{\partial y_i}\right\rangle = -\frac{1}{V}\int_{\mathrm{S_I}} \phi_j^{(k)}(\boldsymbol{y},t) n_{ki}\mathrm{d}S(\boldsymbol{y}), \tag{9}$$

where ϕ_j denotes an arbitrary quantity.

2.3.1. Additional terms of shear stress

The second term on the right-hand side of Eq. (8) can be approximated as follows:

$$\frac{\partial}{\partial x_j}\left[\alpha_k\overline{\mu_k\left(\frac{\partial u_{ki}}{\partial y_j}+\frac{\partial u_{kj}}{\partial y_i}\right)}\right]\approx\frac{\partial}{\partial x_j}\left[\alpha_k\overline{\mu_k}\left(\frac{\partial\widehat{u_{ki}}}{\partial x_j}+\frac{\partial\widehat{u_{kj}}}{\partial x_i}\right)\right]+\frac{\partial}{\partial x_j}(\alpha_k C_k), \tag{10}$$

where C_k is an additional term determined via the approximation of volume-averaged spatial derivatives. We present the following three cases involving additional terms:

$$C_k=\begin{cases}0 & : \text{Case 1}\\ -\overline{\mu_k}\left(\widehat{u_{ki}}\dfrac{\partial\alpha_k}{\partial x_j}+\widehat{u_{kj}}\dfrac{\partial\alpha_k}{\partial x_i}\right) & : \text{Case 2}\\ -\dfrac{\overline{\mu_k}}{\overline{\rho_k}}\left(\widehat{u_{ki}}\dfrac{\partial\overline{\rho_k}}{\partial x_j}+\widehat{u_{kj}}\dfrac{\partial\overline{\rho_k}}{\partial x_i}\right) & : \text{Case 3}\end{cases} \tag{11}$$

Case 1 used the assumptions $\overline{\partial u_{ki}/\partial y_j}\approx\partial\overline{u_{ki}}/\partial x_j$ and $\overline{u_{ki}}\approx\widehat{u_{ki}}$. Most studies have adopted the parameters in case 1 because the contribution of the additional term is small when the typical dimension of V is sufficiently larger than the bubble size (Brennen, 2005). Case 2 used the assumptions $\overline{\partial u_{ki}/\partial y_j}\approx\partial\overline{u_{ki}}/\partial x_j$, $\overline{u_{ki}}\approx\widehat{u_{ki}}$, and the following relation for the phase-averaged spatial derivative (Brennen, 2005):

$$\overline{\frac{\partial\phi_{ki}}{\partial y_j}}=\frac{\partial\overline{\phi_{ki}}}{\partial x_j}+\frac{1}{\alpha_k V}\int_{S_I}\phi_i^{(k)}n_{kj}\mathrm{d}S, \tag{12}$$

and $u_i^{(k)}\approx\widehat{u_{ki}}$, The last assumption implies that the boundary-layer thickness is ignored and that the integral of Eq. (12) can be transformed using the Slattery's theorem (see Section 2.3.2). Case 3 used the assumptions $\overline{\partial u_{ki}/\partial y_j}\approx\widehat{\partial u_{ki}/\partial y_j}$, $u_i^{(k)}\approx\widehat{u_{ki}}$, and the mass-weighted relation of the phase-averaged spatial derivative:

$$\widehat{\frac{\partial u_{ki}}{\partial y_j}}\approx\frac{\partial\widehat{u_{ki}}}{\partial x_j}-\frac{\widehat{u_{ki}}}{\overline{\rho_k}}\frac{\partial\overline{\rho_k}}{\partial x_j}. \tag{13}$$

2.3.2. Interfacial pressure term in liquid

In this section, we describe the transformation of the forth term of the right-hand side in Eq. (8) (Egashira et al., 2004). The non-averaged liquid pressure $p^{(\mathrm{L})}$ can be decomposed into the following three parts:

$$p^{(\mathrm{L})}(\boldsymbol{x};\boldsymbol{y},t) = \overline{p_{\mathrm{L}}}(\boldsymbol{x},t) + \widetilde{P}(\boldsymbol{x},t) + p_f(\boldsymbol{y},t), \tag{14}$$

where $\widetilde{P}$ denotes the surface-averaged deviation that is given as follows:

$$\widetilde{P}(\boldsymbol{x},t) = \frac{1}{S_I}\int_{\mathrm{S_I}} \big(p^{(\mathrm{L})}(\boldsymbol{x};\boldsymbol{y},t) - \overline{p_{\mathrm{L}}}(\boldsymbol{x},t)\big)\mathrm{d}S(\boldsymbol{y}), \tag{15}$$

and p_f is the deviation of $p^{(\mathrm{L})}$ from $\overline{p_{\mathrm{L}}} + \widetilde{P}$.

Bubbles in the control volume can be classified into two types (Prosperetti and Jones, 1984): bubbles that are completely contained in the control volume V and bubbles that are cut across the surface of the control volume S (Fig. 1 (a)). Figure 1 (a) also illustrates that the surface S can be divided into two parts: S_{L} is the surface S comprising the liquid and S_{G} is the surface S comprising the gas (Prosperetti and Jones, 1984; Egashira et al., 2004). Because the union of S_I and S_{G} forms a set of closed surfaces, we can show the following relation for the normal stress of the bubble $n_i = n_{\mathrm{G}i} = -n_{\mathrm{L}i}$:

$$\int_{S_I} n_i \,\mathrm{d}S + \int_{S_{\mathrm{G}}} n_i \,\mathrm{d}S = 0. \tag{16}$$

According to the Slattery's theorem (Slattery, 1967; Whiaker, 1969), we have

$$\int_{S_{\mathrm{G}}} n_i \,\mathrm{d}S = \frac{\partial}{\partial x_i}\int_{V_{\mathrm{G}}} \mathrm{d}V. \tag{17}$$

Using Eqs. (14), (16), and (17) into Eq. (8), we obtained the interfacial pressure term in the liquid phase as follows:

$$-\frac{1}{V}\int_{S_I} p^{(\mathrm{L})} n_{\mathrm{L}i} \,\mathrm{d}S = -\Big(\overline{p_{\mathrm{L}}} + \widetilde{P}\Big)\frac{\partial \alpha_{\mathrm{G}}}{\partial x_i} + \frac{1}{V}\int_{S_I} p_f n_i \,\mathrm{d}S. \tag{18}$$

The second term on the right-hand side of Eq. (18) represents the total force acting on all bubbles in V and is regarded as the virtual mass force F_i^{VM} acting on all bubbles in V. Several virtual mass-force models were proposed (e.g. Drew et al., 1979; Drew, 1983; Ishii and Mishima, 1980; Kameda and

Matsumoto, 1996), and we employed the following models incorporating the liquid compressibility (Zhang and Prosperetti, 1994; Eames and Hunt, 2004; Yano et al., 2006):

$$F_i^{\mathrm{VM}} = -\beta_1 \alpha_{\mathrm{G}} \overline{\rho_{\mathrm{L}}} \left(\frac{D_{\mathrm{G}} \widehat{u_{\mathrm{G}i}}}{Dt} - \frac{D_{\mathrm{L}} \widehat{u_{\mathrm{L}i}}}{Dt} \right) - \beta_2 \overline{\rho_{\mathrm{L}}} (\widehat{u_{\mathrm{G}i}} - \widehat{u_{\mathrm{L}i}}) \frac{D_{\mathrm{G}} \alpha_{\mathrm{G}}}{Dt} - \beta_3 \alpha_{\mathrm{G}} (\widehat{u_{\mathrm{G}i}} - \widehat{u_{\mathrm{L}i}}) \frac{D_{\mathrm{G}} \overline{\rho_{\mathrm{L}}}}{Dt}, \tag{19}$$

where $\beta_i \, (i = 1, 2, 3)$ is set to $1/2$ for spherical bubbles.

2.3.3. Interfacial shear stress term in the liquid

Let the integrand of the fifth term on the right-hand side of Eq. (8) be

$$\tau_{ij}^{(k)} = \left[\mu \left(\frac{\partial u_i}{\partial x_j} + \frac{\partial u_j}{\partial x_i} \right) \right]^{(k)}, \tag{20}$$

and $\tau_{ij}^{(\mathrm{L})}$ can be decomposed into

$$\tau_{ij}^{(\mathrm{L})} = \overline{\tau_{\mathrm{L}ij}}(\boldsymbol{x}, t) + \tau_{fij}(\boldsymbol{y}, t), \tag{21}$$

where $\overline{\tau_{\mathrm{L}ij}}$ denotes the volume-averaged shear stress tensor in the liquid phase, which is equal to the additional term (11) that is given as,

$$\overline{\tau_{\mathrm{L}ij}} \approx \mu_{\mathrm{L}} \left(\frac{\partial \widehat{u_{\mathrm{L}i}}}{\partial x_j} + \frac{\partial \widehat{u_{\mathrm{L}j}}}{\partial x_i} \right) + C_{\mathrm{L}}, \tag{22}$$

and τ_{fij} denotes the deviation of $\tau_{ij}^{(\mathrm{L})}$ from $\overline{\tau_{\mathrm{L}ij}}$. Substituting Eqs. (17) and (21) with Eq. (8), we obtained the interfacial shear stress term in the liquid phase as follows:

$$\frac{1}{V} \int_{S_I} \tau_{ij}^{(\mathrm{L})} n_{\mathrm{L}j} \mathrm{d}S = \overline{\tau_{\mathrm{L}ij}} \frac{\partial \alpha_{\mathrm{G}}}{\partial x_j} - \frac{1}{V} \int_{S_I} \tau_{fij} n_j \mathrm{d}S. \tag{23}$$

The second term on the right-hand side of Eq. (23) represents the total shear force acting on all bubbles in V. This term encompasses the drag force (Ishii and Zuber, 1979), lift force (Ẑun, 1980), and wall lubrication force (Antal et al., 1991). Nonetheless, this study considered only the drag force, which can be modelled as,

$$F_i^{\mathrm{DR}} = -\frac{3}{8R} C_D \alpha_{\mathrm{G}} \overline{\rho_{\mathrm{L}}} (\widehat{u_{\mathrm{G}i}} - \widehat{u_{\mathrm{L}i}}) \, |\widehat{u_{\mathrm{G}i}} - \widehat{u_{\mathrm{L}i}}|, \tag{24}$$

where C_D is the drag coefficient. Although there are various drag coefficient models for different flow conditions (Levich, 1962; Schiller and Naumann, 1933; Ishii and Zuber, 1979; Tomiyama et al., 1998), we select no specific drag coefficient models to ensure generality.

2.3.4. Momentum conservations for gas and liquid

The momentum balance equation at the interface, without considering the mass transportation (Ishii and Hibiki, 2010) was given as,

$$-\left(-p^{(\mathrm{G})}\delta_{ij}+\tau_{ij}^{(\mathrm{G})}\right)n_{\mathrm{G}j}-\left(-p^{(\mathrm{L})}\delta_{ij}+\tau_{ij}^{(\mathrm{L})}\right)n_{\mathrm{L}j}+\frac{2\sigma}{R}n_{\mathrm{L}i}+\frac{4\mu_{\mathrm{L}}}{R}\frac{\partial R}{\partial t}n_{\mathrm{L}i}=0. \tag{25}$$

Combining Eq. (25) with S_I, dividing by V, and using Eqs. (17), (18), and (23), we obtained the following interfacial terms for the gas phase:

$$-\frac{1}{V}\int_{\mathrm{S_I}}p^{(\mathrm{G})}n_i^{\mathrm{I}}\mathrm{d}S+\frac{1}{V}\int_{\mathrm{S_I}}\tau_{ij}^{(\mathrm{G})}n_j^{\mathrm{I}}\mathrm{d}S=\overline{p_{\mathrm{G}}}\frac{\partial\alpha_{\mathrm{G}}}{\partial x_i}-\overline{\tau_{\mathrm{L}ij}}\frac{\partial\alpha_{\mathrm{G}}}{\partial x_j}+F_i^{\mathrm{VM}}+F_i^{\mathrm{DR}}. \tag{26}$$

We regarded the interfacial shear force as the volume-averaged liquid shear stress in both phases, and this approximation is consistent with that given in Ishii and Hibiki (2010). By contrast, Antal et al. (1991) neglected interfacial shear stress in the gas phase (Chuang and Hibiki, 2017).

Finally, the momentum conservations in the gas and liquid can be defined as,

$$\begin{aligned}&\frac{\partial}{\partial t}(\alpha_{\mathrm{G}}\overline{\rho_{\mathrm{G}}}\widehat{u_{\mathrm{G}i}})+\frac{\partial}{\partial x_j}(\alpha_{\mathrm{G}}\overline{\rho_{\mathrm{G}}}\widehat{u_{\mathrm{G}i}}\widehat{u_{\mathrm{G}j}})\\&=-\alpha_{\mathrm{G}}\frac{\partial\overline{p_{\mathrm{G}}}}{\partial x_i}+\frac{\partial}{\partial x_j}\left[\alpha_{\mathrm{G}}\overline{\mu_{\mathrm{G}}}\left(\frac{\partial\widehat{u_{\mathrm{G}i}}}{\partial x_j}+\frac{\partial\widehat{u_{\mathrm{G}j}}}{\partial x_i}\right)\right]+\frac{\partial}{\partial x_j}(\alpha_{\mathrm{G}}C_{\mathrm{G}})-\overline{\tau_{\mathrm{L}ij}}\frac{\partial\alpha_{\mathrm{G}}}{\partial x_j}\\&\quad+F_i^{\mathrm{VM}}+F_i^{\mathrm{DR}},\end{aligned} \tag{27}$$

and

$$\begin{aligned}&\frac{\partial}{\partial t}(\alpha_{\mathrm{L}}\overline{\rho_{\mathrm{L}}}\widehat{u_{\mathrm{L}i}})+\frac{\partial}{\partial x_j}(\alpha_{\mathrm{L}}\overline{\rho_{\mathrm{L}}}\widehat{u_{\mathrm{L}i}}\widehat{u_{\mathrm{L}j}})\\&=-\alpha_{\mathrm{L}}\frac{\partial\overline{p_{\mathrm{L}}}}{\partial x_i}+\alpha_{\mathrm{L}}\mu_{\mathrm{L}}\frac{\partial}{\partial x_j}\left(\frac{\partial\widehat{u_{\mathrm{L}i}}}{\partial x_j}+\frac{\partial\widehat{u_{\mathrm{L}j}}}{\partial x_i}\right)+\alpha_{\mathrm{L}}\frac{\partial C_{\mathrm{L}}}{\partial x_j}-\widetilde{P}\frac{\partial\alpha_{\mathrm{G}}}{\partial x_i}-F_i^{\mathrm{VM}}-F_i^{\mathrm{DR}},\end{aligned} \tag{28}$$

where $C_k\,(k=\mathrm{G},\mathrm{L})$, $\overline{\tau_{\mathrm{L}ij}}$, F^{VM}, and F^{DR} are defined as Eqs. (11), (22), (19), and (24), respectively.

2.4. Energy conservation

The single-phase energy conservation for a Newtonian fluid is given as,

$$\begin{aligned}&\frac{\partial}{\partial t}\left[\rho\left(\frac{u_i^2}{2}+e\right)\right]+\frac{\partial}{\partial y_j}\left[\rho\left(\frac{u_i^2}{2}+e\right)u_j\right]\\=&\frac{\partial}{\partial y_j}\left[-p\delta_{ij}u_i+\mu\left(\frac{\partial u_i}{\partial y_j}+\frac{\partial u_j}{\partial y_i}\right)u_i\right]-\frac{\partial Q_j}{\partial y_j},\end{aligned}\tag{29}$$

where e and Q_j denote the internal energy and heat flux per unit mass, respectively. The external forces were ignored. According to Fourier's law, the heat flux Q_j can be expressed as $-\lambda\,\partial T/\partial y_j$, where λ and T are the thermal conductivity and temperature, respectively. In this study, λ was assumed to be constant. Based on Eqs. (1)–(4) and Eq. (9), the energy conservation in the k-th phase becomes

$$\begin{aligned}&\frac{\partial}{\partial t}\left[\alpha_k\overline{\rho_k}\left(\widehat{\frac{u_{ki}^2}{2}}+\widehat{e_k}\right)\right]+\frac{\partial}{\partial x_j}\left[\alpha_k\overline{\rho_k}\left(\widehat{\frac{u_{ki}^2u_{kj}}{2}}+\widehat{e_ku_{kj}}\right)\right]\\=&-\frac{\partial}{\partial x_i}(\alpha_k\overline{p_ku_{kj}})+\frac{\partial}{\partial x_j}\left[\overline{\alpha_k\mu_k\left(\frac{\partial u_{ki}}{\partial x_j}+\frac{\partial u_{kj}}{\partial x_i}\right)u_{ki}}\right]+\frac{\partial^2}{\partial x_j^2}(\alpha_k\lambda_k\overline{T_k})\\&-\frac{1}{V}\int_{S_I}[pu_i]^{(k)}n_{ki}\mathrm{d}S+\frac{1}{V}\int_{S_I}\left[\mu\left(\frac{\partial u_i}{\partial y_j}+\frac{\partial u_j}{\partial y_i}\right)u_i\right]^{(k)}n_{kj}\mathrm{d}S\\&+2\lambda_k\frac{1}{V}\int_{S_I}\left[\frac{\partial T}{\partial y_j}\right]^{(k)}n_{kj}\mathrm{d}S-\left\langle\lambda T\frac{\partial^2X_k}{\partial y_j^2}\right\rangle.\end{aligned}\tag{30}$$

2.4.1. Transformation of interfacial terms

We assumed that the average quantities of the product of the physical quantities in Eq. (30) can be decomposed as follows:

$$\begin{aligned}&\widehat{u_{ki}^2}\approx\widehat{u_{ki}}^2,\quad\widehat{u_{ki}^2u_{kj}}\approx\widehat{u_{ki}}^2\widehat{u_{kj}},\quad\widehat{e_ku_{kj}}\approx\widehat{e_k}\widehat{u_{kj}},\quad\overline{p_ku_{kj}}\approx\overline{p_k}\widehat{u_{kj}},\\&\overline{\mu_k\left(\frac{\partial u_{ki}}{\partial y_j}+\frac{\partial u_{kj}}{\partial y_i}\right)u_{kj}}\approx\overline{\mu_k}\left(\frac{\partial\widehat{u_{ki}}}{\partial x_j}+\frac{\partial\widehat{u_{kj}}}{\partial x_i}\right)\widehat{u_{kj}}+C_k\widehat{u_{kj}}.\end{aligned}\tag{31}$$

The fourth and fifth terms on the right-hand side of Eq. (30) can be approximated as follows:

$$-\frac{1}{V}\int_{\mathrm{S_I}}[pu_i]^{(k)}n_{ki}\mathrm{d}S \approx -\widehat{u_{ki}}\frac{1}{V}\int_{\mathrm{S_I}}p^{(k)}n_{ki}\mathrm{d}S, \tag{32}$$

$$\frac{1}{V}\int_{\mathrm{S_I}}\left[\mu\left(\frac{\partial u_i}{\partial y_j}+\frac{\partial u_j}{\partial y_i}\right)u_i\right]^{(k)}n_{kj}\mathrm{d}S \approx \widehat{u_{ki}}\frac{1}{V}\int_{\mathrm{S_I}}\left[\mu\left(\frac{\partial u_i}{\partial y_j}+\frac{\partial u_j}{\partial y_i}\right)\right]^{(k)}n_{kj}\mathrm{d}S, \tag{33}$$

based on the assumption $u_i^{(k)}(\boldsymbol{y},t)\approx\widehat{u_{ki}}(\boldsymbol{x},t)$.

The seventh term on the right-hand side of Eq. (30) involves the second-order derivatives of the phase indicator function X_k. Herein, we discuss the transformation of this term. Using Eqs. (1), (2), and Gauss's theorem, we obtained the generalised form of the term as follows:

$$\left\langle\phi_j(\boldsymbol{y},t)\frac{\partial}{\partial y_i}\frac{\partial X_k(\boldsymbol{y},t)}{\partial y_j}\right\rangle = \frac{1}{V}\oint_{\mathrm{S}}\phi_j\frac{\partial X_k}{\partial y_j}n_i\mathrm{d}S+\frac{1}{V}\int_{\mathrm{S_I}}\left[\frac{\partial\phi_j}{\partial y_i}\right]^{(k)}n_{kj}\mathrm{d}S. \tag{34}$$

Because the derivative of the phase indicator function $\partial X_k/\partial y_j$ is equal to the delta function $\delta(\boldsymbol{y}-\boldsymbol{y}^{\mathrm{I}})n_{kj}$ ($\boldsymbol{y}^{\mathrm{I}}$ is the position of the gas–liquid interface) (Drew, 1983), the first term on the right-hand side of Eq. (34) can be rewritten as,

$$\frac{1}{V}\oint_{S}\phi_j\frac{\partial X_k}{\partial y_j}n_i\mathrm{d}S=\frac{1}{V}\oint_{\partial S_{\mathrm{G}}}\phi_j n_{kj}r_i\mathrm{d}s(\boldsymbol{y}), \tag{35}$$

where ∂S_{G} is the boundary of S_{G} and r_i is the differential arc length on ∂S_{G} (Fig. 1 (c)). The contribution of Eq. (35) is exceedingly small compared with the second term on the right-hand side of Eq. (34) because the bubbles are sufficiently far apart that their interaction can be considered to be negligible. Therefore, we approximated Eq. (34) as follows:

$$\left\langle\phi_j(\boldsymbol{y},t)\frac{\partial}{\partial y_i}\frac{\partial X_k(\boldsymbol{y},t)}{\partial y_j}\right\rangle \approx \frac{1}{V}\int_{\mathrm{S_I}}\left[\frac{\partial\phi_j}{\partial y_i}\right]^{(k)}n_{kj}\mathrm{d}S. \tag{36}$$

Based on the conservation equations of mass and momentum in the k-th

phase and Eq. (36), the thermal energy equation in the k-th phase becomes

$$\begin{aligned}
&\alpha_k\overline{\rho_k}\frac{\partial\widehat{e_k}}{\partial t}+\alpha_k\overline{\rho_k}\widehat{u_{kj}}\frac{\partial\widehat{e_k}}{\partial x_j}\\
=&-\alpha_k\overline{p_k}\frac{\partial\widehat{u_{ki}}}{\partial x_i}+\alpha_k\overline{\mu_k}\left(\frac{\partial\widehat{u_{ki}}}{\partial x_j}+\frac{\partial\widehat{u_{kj}}}{\partial x_i}\right)\frac{\partial\widehat{u_{ki}}}{\partial x_j}+\alpha_k C_k\frac{\partial\widehat{u_{ki}}}{\partial x_j}+\frac{\partial^2}{\partial x_j^2}\left(\alpha_k\lambda_k\overline{T_k}\right)\\
&+\lambda_k\frac{1}{V}\int_{\mathrm{S_I}}\left[\frac{\partial T}{\partial y_j}\right]^{(k)}n_{kj}\mathrm{d}S. \qquad (37)
\end{aligned}$$

2.4.2. Temperature gradient at gas-liquid interface

Equation (37) can describe not only the bubbly flows but also the general two-phase flows such as mist and particle flows. Closing the last term of the right-hand side via constitutive equations for a single bubble can limit Eq. (37) to that for bubbly flow.

First, we focus on the thermal energy equation in the gas. The mass-weighted phase-averaged internal energy becomes $\widehat{e_{\mathrm{G}}}=c_V\overline{T_{\mathrm{G}}}$ based on the assumption of an ideal gas, where c_V is the specific heat at a constant volume (Ishii and Hibiki, 2010). Because the bubbles are spherical and $n_{\mathrm{G}j}$ is the normal vector in the outward direction from the bubble at the interface, we rewrote the integrand of the last term in Eq. (37) as,

$$\left[\frac{\partial T}{\partial y_j}\right]^{(\mathrm{G})}n_{\mathrm{G}j}=\left.\frac{\partial T}{\partial r}\right|_{r=R(\boldsymbol{x},t)}, \qquad (38)$$

where r is the polar coordinate, with the bubble center as the origin, and $R(\boldsymbol{x},t)$ is the uniform bubble radius within V. Therefore, the right-hand side of Eq. (38) depends only on global spatial coordinate $\boldsymbol{x}$. Using Eq. (38) and the relation $S_I/V=3\alpha_{\mathrm{G}}/R$, we obtained

$$\lambda_{\mathrm{G}}\frac{1}{V}\int_{\mathrm{S_I}}\left[\frac{\partial T}{\partial y_j}\right]^{(\mathrm{G})}n_{\mathrm{G}j}\mathrm{d}S=\lambda_{\mathrm{G}}\left.\frac{\partial T}{\partial r}\right|_{r=R(\boldsymbol{x},t)}\frac{3\alpha_{\mathrm{G}}}{R}. \qquad (39)$$

We assume that the interfacial thermal energy (39) is split into the two parts as

$$\left.\frac{\partial T}{\partial r}\right|_{r=R(\boldsymbol{x},t)}=\left.\frac{\partial T}{\partial r}\right|^{\mathrm{TC}}_{r=R(\boldsymbol{x},t)}+\left.\frac{\partial T}{\partial r}\right|^{\mathrm{HT}}_{r=R(\boldsymbol{x},t)}, \qquad (40)$$

where the first and second terms represent the effects of the thermal conduction and the heat transfer, respectively.

The first term of Eq. (40) can be closed by the two alternatives. First, the relation between the differential equation for the gas pressure as

$$\frac{D_{\mathrm{G}}\overline{p_{\mathrm{G}}}}{Dt} = \frac{3}{R}\left[(\kappa-1)\lambda_{\mathrm{G}}\left.\frac{\partial T}{\partial r}\right|_{r=R}^{\mathrm{TC}} - \kappa\overline{p_{\mathrm{G}}}\frac{D_{\mathrm{G}}R}{Dt}\right], \tag{41}$$

where κ is the heat capacity ratio. This relation is derived from the energy equation for a single bubble near the interface using the assumption of uniform temperature distributions (Nigmatulin et al., 1981; Prosperetti et al., 1988; Prosperetti, 1991). Second, the models of temperature gradient at the interface, which were introduced to evaluate the temperature gradient term of Eq. (41) using the average temperature value inside the bubbles instead of solving the energy equation that describes temperature distributions inside the bubbles, as

$$\left.\frac{\partial T}{\partial r}\right|_{r=R}^{\mathrm{TC}} = \begin{cases} \dfrac{T_{\mathrm{I}}-\overline{T_{\mathrm{G}}}}{\sqrt{2\pi D/\omega_{\mathrm{B}}}} & : \text{LSM model} \\ \dfrac{T_{\mathrm{I}}-\overline{T_{\mathrm{G}}}}{|\tilde{L}_p|} & : \text{PCB model} \\ \dfrac{\mathrm{Re}(\tilde{L}_p)(T_{\mathrm{I}}-\overline{T_{\mathrm{G}}})}{|\tilde{L}_p|^2} + \dfrac{\mathrm{Im}(\tilde{L}_p)}{\omega_{\mathrm{B}}|\tilde{L}_p|^2}\dfrac{\partial T_{\mathrm{G}}}{\partial t} & : \text{STM model} \end{cases} \tag{42}$$

The LSM model (Lertnuwat et al., 2001) was derived by estimating the thermal penetration length inside a bubble, the PCB model (Preston et al., 2002) was strictly derived using the linear theory, and the STM model (Sugiyama et al., 2005a,b) was derived by incorporating a phase difference between the temperature gradient and the temperature inside a bubble based on the PCB model. In Eq. (42), D is the thermal diffusivity and T_{I} is the temperature of the gas–liquid interface. This study regarded T_{I} as the constant liquid temperature T_{L}. The angular frequency of bubble oscillations ω_{B} and $\tilde{L}_p$ were defined as follows (Preston et al., 2002; Sugiyama et al., 2005a):

$$\omega_{\mathrm{B}} = \left[\frac{3\gamma_e p_{\mathrm{G}0} - 2\sigma/R_0}{\rho_{\mathrm{L}0}R_0} - \left(\frac{2\mu_{e0}}{\rho_{\mathrm{L}0}{R_0}^2}\right)^2\right]^{1/2}, \tag{43}$$

$$\widetilde{L}_p = \frac{R_0(\alpha_{\mathrm{N}}^2 - 3\alpha_{\mathrm{N}}\coth\alpha_{\mathrm{N}} + 3)}{\alpha_{\mathrm{N}}^2(\alpha_{\mathrm{N}}\coth\alpha_{\mathrm{N}} - 1)}, \tag{44}$$

where

$$\gamma_e = \mathrm{Re}\left(\frac{\Gamma_\mathrm{N}}{3}\right), \quad \mu_{e0} = \mu_\mathrm{L} + \mathrm{Im}\left(\frac{p_{\mathrm{G}0}\Gamma_\mathrm{N}}{4\omega_\mathrm{B}}\right)$$
$$\Gamma_\mathrm{N} = \frac{3\alpha_\mathrm{N}^2\gamma}{\alpha_\mathrm{N}^2 + 3(\gamma-1)(\alpha_\mathrm{N}\coth\alpha_\mathrm{N} - 1)}, \quad \alpha_\mathrm{N} = (1+\mathrm{i})\left(\frac{\gamma\omega_\mathrm{B}p_{\mathrm{G}0}{R_0}^2}{2(\gamma-1)T_{\mathrm{G}0}\kappa_\mathrm{G}}\right)^{1/2}. \tag{45}$$

The second term of Eq. (40) can be closed by the thermal energy equation in the liquid. The averaged internal energy became (Ishii and Hibiki, 2010)

$$\mathrm{d}\widehat{e}_\mathrm{L} = c_{p\mathrm{L}}\mathrm{d}\overline{T}_\mathrm{L} + \frac{1}{\overline{\rho}_\mathrm{L}}\left(1+\beta_\mathrm{L}\overline{T}_\mathrm{L}\right)\mathrm{d}\overline{p}_\mathrm{L} + \frac{\overline{p}_\mathrm{L}}{\overline{\rho}_\mathrm{L}^2}\mathrm{d}\overline{\rho}_\mathrm{L} - \frac{1}{\overline{\rho}_\mathrm{L}}\mathrm{d}\overline{p}_\mathrm{L}, \tag{46}$$

where β_L is the coefficient of thermal expansion. As well as Eq. (39), we rewrote the last term in Eq. (37) for the liquid as

$$\lambda_\mathrm{L}\frac{1}{V}\int_{\mathrm{S_I}}\left[\frac{\partial T}{\partial y_j}\right]^{(\mathrm{L})} n_{\mathrm{L}j}\mathrm{d}s = -\lambda_\mathrm{L}\left.\frac{\partial T_\mathrm{L}}{\partial r}\right|_{r=R}\frac{3\alpha_\mathrm{G}}{R}. \tag{47}$$

The right-hand side in Eq. (47) is equal to the temperature gradient term in the gas (39) by using the energy balance between the two phases (Fuster and Montel, 2015; Warnez and Johnsen, 2015)

$$\lambda_\mathrm{G}\left.\frac{\partial T_\mathrm{G}}{\partial r}\right|_{r=R}^{\mathrm{HT}} = \lambda_\mathrm{L}\left.\frac{\partial T_\mathrm{L}}{\partial r}\right|_{r=R}. \tag{48}$$

Substituting Eqs. (46),(47),(48) into Eq. (37), we obtained the thermal energy equation in the liquid as

$$\begin{aligned}
&\alpha_\mathrm{L}(1+\beta_\mathrm{L}T_\mathrm{L})\frac{\partial\overline{p}_\mathrm{L}}{\partial t} + \alpha_\mathrm{L}\frac{\overline{p}_\mathrm{L}}{\overline{\rho}_\mathrm{L}}\frac{\partial\overline{\rho}_\mathrm{L}}{\partial t} - \alpha_\mathrm{L}\frac{\partial\overline{p}_\mathrm{L}}{\partial t} \\
&+ \alpha_\mathrm{L}(1+\beta_\mathrm{L}T_\mathrm{L})u_{\mathrm{L}j}\frac{\partial\overline{p}_\mathrm{L}}{\partial x_j} + \alpha_\mathrm{L}\frac{\overline{p}_\mathrm{L}}{\overline{\rho}_\mathrm{L}}u_{\mathrm{L}j}\frac{\partial\overline{\rho}_\mathrm{L}}{\partial x_j} - \alpha_\mathrm{L}u_{\mathrm{L}j}\frac{\partial\overline{p}_\mathrm{L}}{\partial x_j} \\
=& -\alpha_\mathrm{L}\overline{p}_\mathrm{L}\frac{\partial\widehat{u}_{\mathrm{L}j}}{\partial x_j} + \alpha_\mathrm{L}\mu_\mathrm{L}\left(\frac{\partial\widehat{u}_{\mathrm{L}i}}{\partial x_j} + \frac{\partial\widehat{u}_{\mathrm{L}j}}{\partial x_i}\right)\frac{\partial\widehat{u}_{\mathrm{L}i}}{\partial x_j} + \alpha_\mathrm{L}C_\mathrm{L}\frac{\partial\widehat{u}_{\mathrm{L}i}}{\partial x_j} + \lambda_\mathrm{L}T_\mathrm{L}\frac{\partial\widehat{u}_{\mathrm{L}i}}{\partial x_j} \\
&+ \lambda_\mathrm{L}T_\mathrm{L}\frac{\partial^2\alpha_\mathrm{L}}{\partial x_j^2} - \lambda_\mathrm{G}\left.\frac{\partial T_\mathrm{G}}{\partial r}\right|_{r=R}^{\mathrm{HT}}\frac{3\alpha_\mathrm{G}}{R}.
\end{aligned} \tag{49}$$

A simple form of the energy equation is commonly used to focusing a practical importance if the Eckert numbers are very small, or the heat transfer dominants the energy exchanges (Ishii and Hibiki, 2010). From this assumption, Eq. (49) can be simplified as

$$0 = \lambda_{\mathrm{L}} T_{\mathrm{L}} \frac{\partial^2 \alpha_{\mathrm{L}}}{\partial x_j^2} - \lambda_{\mathrm{G}} \left. \frac{\partial T_{\mathrm{G}}}{\partial r} \right|_{r=R}^{\mathrm{HT}} \frac{3\alpha_{\mathrm{G}}}{R}. \tag{50}$$

Finally, the energy conservation in the gas becomes

$$\begin{aligned} & c_{\mathrm{V}} \alpha_{\mathrm{G}} \overline{\rho_{\mathrm{G}}} \frac{\partial \overline{T_{\mathrm{G}}}}{\partial t} + c_{\mathrm{V}} \alpha_{\mathrm{G}} \overline{\rho_{\mathrm{G}}} \widehat{u_{\mathrm{G}j}} \frac{\partial \overline{T_{\mathrm{G}}}}{\partial x_j} \\ = & - \alpha_{\mathrm{G}} \overline{p_{\mathrm{G}}} \frac{\partial \widehat{u_{\mathrm{G}i}}}{\partial x_i} + \alpha_{\mathrm{G}} \overline{\mu_{\mathrm{G}}} \left(\frac{\partial \widehat{u_{\mathrm{G}i}}}{\partial x_j} + \frac{\partial \widehat{u_{\mathrm{G}j}}}{\partial x_i} \right) \frac{\partial \widehat{u_{\mathrm{G}i}}}{\partial x_j} + \alpha_{\mathrm{G}} C_{\mathrm{G}} \frac{\partial \widehat{u_{\mathrm{G}i}}}{\partial x_j} \\ & + \lambda_{\mathrm{G}} \frac{\partial^2}{\partial x_j^2} \left(\alpha_{\mathrm{G}} \overline{T_{\mathrm{G}}} \right) + \lambda_{\mathrm{G}} \left(\left. \frac{\partial T}{\partial r} \right|_{r=R}^{\mathrm{TC}} + \left. \frac{\partial T}{\partial r} \right|_{r=R}^{\mathrm{HT}} \right) \frac{3\alpha_{\mathrm{G}}}{R}, \end{aligned} \tag{51}$$

and the last term is closed by Eqs. (41) or (42), and Eq. (50).

2.5. Closure of two-fluid model equations with bubble oscillations

The conservations of the two-fluid model equations with bubble oscillations include the mass conservations in both phases (6)(7), momentum conservations in both phases (27)(28), and the energy conservation in the gas (51). To close these conservations, we integrated the following constitutive equations into the two-fluid model equations:
the void fraction constraint condition

$$\alpha_{\mathrm{G}} + \alpha_{\mathrm{L}} = 1, \tag{52}$$

the mass conservation equation in a single bubble

$$\frac{\overline{\rho_{\mathrm{G}}}}{\overline{\rho_{\mathrm{G0}}}} = \left(\frac{R_0}{R} \right)^3, \tag{53}$$

the state equation in the gas phase

$$\frac{\overline{p_{\mathrm{G}}}}{\overline{p_{\mathrm{G0}}}} = \frac{\overline{\rho_{\mathrm{G}}}}{\overline{\rho_{\mathrm{G0}}}} \frac{\overline{T_{\mathrm{G}}}}{\overline{T_{\mathrm{G0}}}}, \tag{54}$$

the state equation in the liquid phase (Tait equation)

$$\frac{\overline{p_{\mathrm{L}}}+B}{\overline{p_{\mathrm{L0}}}+B}=\left(\frac{\overline{\rho_{\mathrm{L}}}}{\overline{\rho_{\mathrm{L0}}}}\right)^{n} \tag{55}$$

the viscosity in the gas phase (Sutherland's law)

$$\overline{\mu_{\mathrm{G}}}=\overline{\mu_{\mathrm{G0}}}\left(\frac{\overline{T_{\mathrm{G}}}}{\overline{T_{\mathrm{G0}}}}\right)^{\frac{3}{2}}\frac{\overline{T_{\mathrm{G0}}}+C}{\overline{T_{\mathrm{G}}}+C}, \tag{56}$$

the radial equation of motion for an isolated bubble (Keller and Kolodner, 1956)

$$\begin{aligned}&\left(1-\frac{1}{c_{\mathrm{L0}}}\frac{\partial R}{\partial t}\right)R\frac{\partial^2 R}{\partial t^2}+\frac{3}{2}\left(1-\frac{1}{3c_{\mathrm{L0}}}\frac{\partial R}{\partial t}\right)\left(\frac{\partial R}{\partial t}\right)^2\\ =&\left(1+\frac{1}{c_{\mathrm{L0}}}\frac{\partial R}{\partial t}\right)\frac{\widetilde{P}}{\overline{\rho_{\mathrm{L0}}}}+\frac{R}{\overline{\rho_{\mathrm{L0}}}c_{\mathrm{L0}}}\frac{\partial}{\partial t}\left(\overline{p_{\mathrm{L}}}+\widetilde{P}\right),\end{aligned} \tag{57}$$

and the balance of normal stresses across the gas–liquid interface

$$\overline{p_{\mathrm{G}}}=\overline{p_{\mathrm{L}}}+\widetilde{P}+\frac{2\sigma}{R}+\frac{4\mu_{\mathrm{L}}}{R}\frac{\partial R}{\partial t}, \tag{58}$$

where c_{L0} is the speed of sound in the initial unperturbed pure water, n and B are the constants equal to 7.15 and 304.9 for water, respectively, and C is the Sutherland coefficient, which is equal to 117 K for air at 293.15 K. A subscript of 0 represents the initial value.

A feature of our two-fluid model equations is that incorporating the viscosity and the energy conservation allows us to account for the damping of bubble oscillations. Since the earlier model (Egashira et al., 2004) had not considered both the viscosity and thermal effects, the earlier model led to an unphysical result of permanent oscillations of bubbles. Our proposed two-fluid model equations lead to more stable and physically valid solutions, and this is illustrated in Fig. 5 of section 3.

3. Linear dispersion analysis

In this section, we discuss the dynamic behavior of the proposed two-fluid model equations, which comprise Eqs. (6)(7)(27)(28)(51), and (52)–(58), using the linear dispersion analysis. The linear dispersion analysis mathematically evaluate the behavior of small perturbations from a steady state and is

generally used to guarantee the stability of model equations by analyzing the amplification rate of the practical wavenumber. Ramshaw and Trapp (1978), Pokharna et al. (1997), de Bertodano et al. (2016), Vaidheeswaran et al. (2016), Vaidheeswaran and Lopez de Bertodano (2016, 2017), and Clausse et al. (2022) applied the linear dispersion analysis to the gas–liquid two-fluid model.Another method to evaluate the mathematical property of the two-fluid model is the well-posed analysis (e.g. Lyczkowski et al., 1978; Drew and Passman, 1998; Panicker et al., 2018; Tukhvatullina and Frolov, 2018). This method only focuses on the behavior of the solution with an infinitesimal wavelength, as opposed to the linear dispersion analysis. The two-fluid model for bubbly flows with bubble oscillations cannot analyze solutions with a considerably smaller wavelength because the scale of the control volume is much larger than the bubble radius. Therefore, we investigated the dynamic behavior of our proposed model equations using the linear dispersion analysis but not the well-posed analysis.

We first introduced non-dimensional small perturbations of order $\epsilon \ll 1$ as,

$$
\begin{aligned}
&\alpha_{\mathrm{G}}^{*} = \alpha_{0}^{*}(1+\epsilon\alpha_{1}^{*}), \quad \frac{\widehat{u_{\mathrm{G}}}}{U} = u_{\mathrm{G0}}^{*} + \epsilon u_{\mathrm{G1}}^{*}, \quad \frac{\widehat{u_{\mathrm{L}}}}{U} = u_{\mathrm{L0}}^{*} + \epsilon u_{\mathrm{L1}}^{*}, \\
&\frac{\overline{\rho_{\mathrm{G}}}}{\overline{\rho_{\mathrm{L0}}}} = \rho_{\mathrm{G0}}^{*}(1+\epsilon\rho_{\mathrm{G1}}^{*}), \quad \frac{\overline{\rho_{\mathrm{L}}}}{\overline{\rho_{\mathrm{L0}}}} = 1+\epsilon\rho_{\mathrm{L1}}^{*}, \quad \frac{\overline{T_{\mathrm{G}}}}{\overline{T_{\mathrm{G0}}}} = 1+\epsilon T_{\mathrm{G1}}^{*}, \\
&\frac{\overline{p_{\mathrm{G}}}}{\overline{\rho_{\mathrm{L0}}}U^{2}} = p_{\mathrm{G0}}^{*}(1+\epsilon p_{\mathrm{G1}}^{*}), \quad \frac{\overline{p_{\mathrm{L}}}}{\overline{\rho_{\mathrm{L0}}}U^{2}} = p_{\mathrm{L0}}^{*}(1+\epsilon p_{\mathrm{L1}}^{*}), \quad \frac{\widetilde{P}}{\overline{\rho_{\mathrm{L0}}}U^{2}} = \epsilon P_{1}^{*}, \\
&\frac{R}{R_{0}} = 1+\epsilon R_{1}^{*}, \quad \frac{\overline{\mu_{\mathrm{G}}}}{\overline{\rho_{\mathrm{L0}}}UL} = \mu_{\mathrm{G0}}^{*}(1+\epsilon\mu_{\mathrm{G1}}^{*}),
\end{aligned}
\tag{59}
$$

where the superscript $*$ and subscript 0 denote the non-dimensional and initial state values, respectively, the subscript 1 denotes the perturbations from a steady state, U is the representative speed, and L is the representative length. By using Eq. (59), the linearised present model equations are obtained.

$$
\mathbf{A}^{*}\frac{\partial \boldsymbol{v}^{*}}{\partial t^{*}} + \mathbf{B}^{*}\frac{\partial \boldsymbol{v}^{*}}{\partial x^{*}} + \mathbf{C}^{*}\frac{\partial^{2}\boldsymbol{v}^{*}}{\partial x^{*2}} + \mathbf{D}^{*}\boldsymbol{v}^{*} = \mathbf{0}, \tag{60}
$$

where $t^{*} = t/(L/U)$, $x^{*} = x/L$, $\boldsymbol{v}^{*} = [\alpha_{1}^{*}, u_{\mathrm{G1}}^{*}, u_{\mathrm{L1}}^{*}, p_{\mathrm{L1}}^{*}, T_{\mathrm{G1}}^{*}, R_{1}^{*}, S_{1}^{*}]^{T}$ and $\mathbf{A}^{*}, \mathbf{B}^{*}, \mathbf{C}^{*}, \mathbf{D}^{*}$ are the constant matrixes composed of initial and physical

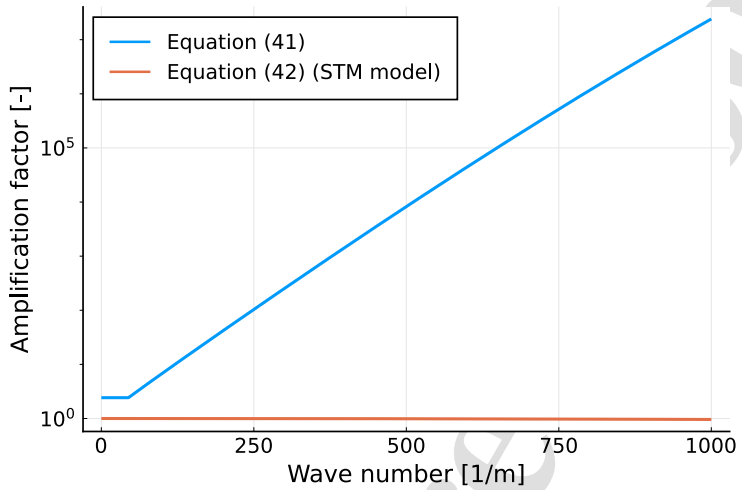

Figure 2: Amplification factor of our proposed model versus the dimensional wavenumber k [1/m] for two cases: the temperature gradient term $\partial T/\partial r\,|^{\mathrm{TC}}_{r=R}$ in Eq. (51) was closed by Eq. (41) or Eq. (42). The STM model (Sugiyama et al., 2005a,b) was used in this figure. The blue and orange curves represent the cases using Eq. (41) and Eq. (42), respectively. The initial and physical parameters are as follows: the initial void fraction $\alpha^*_0 = 0.001$; initial bubble radius $R_0 = 0.1$ [mm]; initial gas velocity $\widehat{u_{\mathrm{G0}}} = 2.5$ [m/s]; initial liquid velocity $\widehat{u_{\mathrm{L0}}} = 2.0$ [m/s]; $\overline{\rho_{\mathrm{G0}}} = 1.206$ [kg/m^3]; $\overline{\rho_{\mathrm{L0}}} = 998.2$ [kg/m^3]; $\overline{p_{\mathrm{G0}}} = 1.013 \times 10^5$ [Pa]; $\overline{p_{\mathrm{L0}}} = 1.013 \times 10^5$ [Pa]; $\overline{T_{\mathrm{G0}}} = 293.15$ [K]; $\overline{\mu_{\mathrm{G0}}} = 1.822 \times 10^{-5}$ [Pa·s]; $\mu_{\mathrm{L}} = 1.002 \times 10^{-3}$ [Pa·s]; $c_{\mathrm{V}} = 1006$ [J/g·K]; $\lambda_{\mathrm{G}} = 0.0257$ [W/m·K]; $\sigma = 0.07275$ [N/m]; and $\kappa^* = 1.4$.

values, which are defined in Appendix A. Substituting the Fourier series expansion of the dependent variable vector $\boldsymbol{v}^*(x^*, t^*) = \sum_{k^*} \hat{\boldsymbol{v}}^*(k^*, t^*)\mathrm{e}^{\theta^* t^*}\mathrm{e}^{\mathrm{i}k^* x^*}$ into Eq. (60), the following generalised eigenvalue problem was obtained:

$$\theta^*(k^*)\mathbf{A}^* = -\mathrm{i}k^*\mathbf{B}^* + {k^*}^2\mathbf{C}^* - \mathbf{D}^*, \tag{61}$$

where k^* is a non-dimensional wavenumber, i is an imaginary unit, and θ^* is an eigenvalue. $\mathrm{Re}\,[\theta^*(k^*)]$ signifies the growth rate of the amplitude of the k^*-th component in $\boldsymbol{v}^*$. Amplitudes grow for positive $\mathrm{Re}\,[\theta^*(k^*)]$, attenuate for negative $\mathrm{Re}\,[\theta^*(k^*)]$, and oscillate within a certain range for a pure imaginary eigenvalue. Amplitude increased by $\left[\mathrm{e}^{\theta^*(k^*)}\right]^{t^*}$ times, which was defined as an amplification factor.

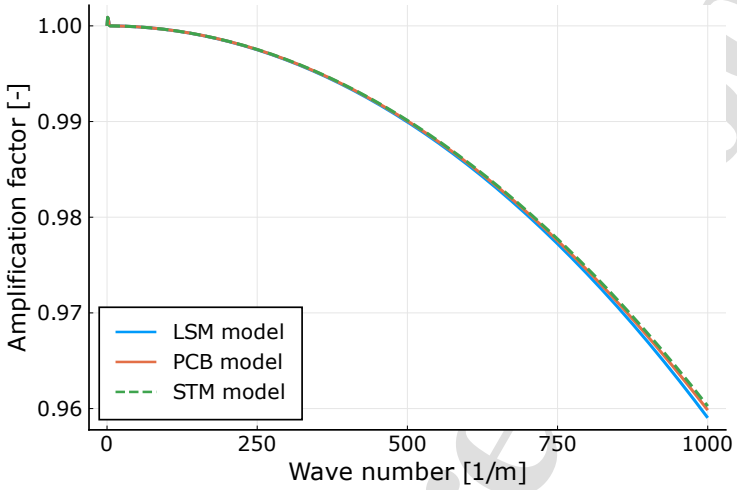

Figure 3: Amplification factors of our proposed model in the case that the temperature gradient term $\partial T/\partial r\,|^{\mathrm{TC}}_{r=R}$ in Eq. (51) was closed by Eq. (42). Blue, orange, and green curves represent the LSM (Lertnuwat et al., 2001), PCB (Preston et al., 2002), and STM models (Sugiyama et al., 2005a), respectively. The initial and physical parameters are the same as those in Fig. 2.

3.1. Temperature gradient at the gas–liquid interface

To reveal the closure of the temperature gradient term $\partial T/\partial r\,|^{\mathrm{TC}}_{r=R}$ in Eq. (51) , Fig. 2 shows the amplification factor of our proposed model equations for using Eq. (41) or Eq. (42) versus the dimensional wavenumber. The initial and physical parameters are shown in the caption of Fig. 2. The dimensional wavenumber k can be obtained from the non-dimensional wavenumber k^* by the relation $k = k^*/(2\pi L)$. The dimensional wavenumber from 0 to 1000 (wavelength from 0.006 m to ∞) was used to cover a range well beyond that of practical numerical interest.

Figure 2 shows that the amplification factor for using Eq. (41) exceed the unity and increased exponentially depending on the wavenumber. This result indicates that initial small perturbations grow instantaneously and that the solutions diverge based on the differential equation for the gas pressure (41) to close the temperature gradient term in the energy conservation. The reason for this instability may be because the spatiotemporal change in the pressure inside the bubbles was evaluated by Eq. (41) and the energy conservation (51). However, the amplification factor for using Eq. (42) represents unity or

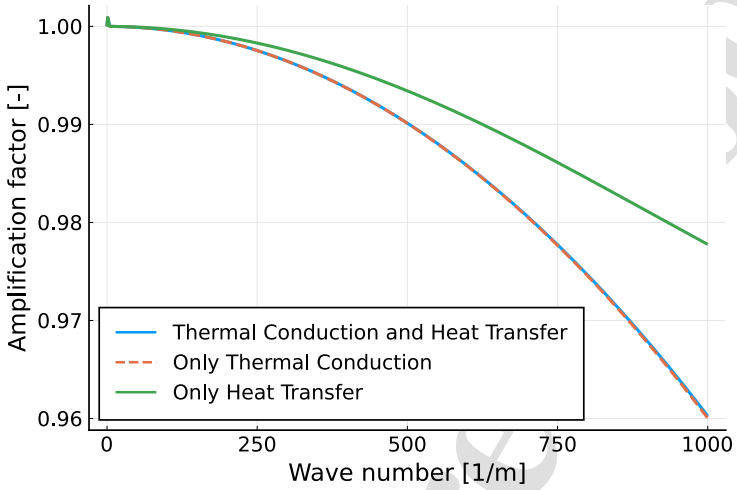

Figure 4: Amplification factors of our proposed model. Blue, orange, and green curves represent the cases considering both the thermal conduction and heat transfer, only the thermal conduction and the heat transfer, respectively. The initial and physical parameters are the same as those in Fig. 2.

less and does not lead to instability because the temperature gradient term was evaluated using only the temperature.

Figure 3 shows the amplification factor depending on the temperature gradient models (42) versus the wavenumber. The initial and physical conditions are the same as those in Fig. 2. As it is obvious from this figure, the effects of the difference in the temperature gradient models on the model stability are small. One of the reasons for this result may be that the linear dispersion analysis does not include non-linear behavior. The STM model is the most accurate model for describing non-linear oscillations of a single bubble (Sugiyama et al., 2005b). The effect of the temperature gradient models may be elucidated by calculating the proposed non-linear two-fluid model equations.

The information in Figs. 2 and 3 reveals that the temperature gradient models at the interface (42) but not the differential equation for the gas pressure (41) should be used to close the temperature gradient term $\partial T/\partial r\,|^{\mathrm{TC}}_{r=R}$ in the energy conservation (51).

To evaluate contributions of the thermal conduction and heat transfer, Fig. 4 shows that the amplification factor of our proposed model equations

considering both the two effects (i.e., $\partial T/\partial r\,|^{\mathrm{TC}}_{r=R} \neq 0$ and $\partial T/\partial r\,|^{\mathrm{HT}}_{r=R} \neq 0$ in Eq. (51)), only the thermal conduction(i.e., $\partial T/\partial r\,|^{\mathrm{TC}}_{r=R} \neq 0$ and $\partial T/\partial r\,|^{\mathrm{HT}}_{r=R} = 0$), and only the heat transfer (i.e., $\partial T/\partial r\,|^{\mathrm{TC}}_{r=R} = 0$ and $\partial T/\partial r\,|^{\mathrm{HT}}_{r=R} \neq 0$) versus the dimensional wavenumber. The blue curve is identical to the green dashed curve in Fig. 3. This figure shows that the green curve is larger than the others at all wavenumbers, and the difference between the blue and orange curves is small. These results indicate that the thermal conduction was dominant in the thermal damping of bubble oscillations in bubbly flows rather than the heat transfer. Damping effects by the thermal conduction, which is proportional to a difference of temperatures between the two phases, is considered to increase in calculating our proposed nonlinear model equations with strong bubble oscillations, because the temperature in gas bubbles becomes high.

3.2. Thermal, bulk viscous, and drag effects

We evaluated the thermal, bulk viscous, and drag effects that are newly incorporated into the proposed model. Figure 5 shows the amplification factor of the proposed model and that of the original two-fluid model (Egashira et al., 2004) versus the dimensional wavenumber. The initial and physical conditions are the same as those in Fig. 2. The purple curve in Fig. 5 is equal to the orange curve in Fig. 2 and the green dashed curve in Fig. 3. The original two-fluid model (the black dashed curve in Fig. 5) corresponds to the proposed model without considering the thermal, bulk viscous, and drag effects. The blue, orange, and green curves represent the proposed model with only the thermal effect (i.e., $\overline{\mu_{\mathrm{G}}}^{*} = 0$, $\mu^{*}_{\mathrm{L}} = 0$, and $C_D = 0$), thermal and drag effects (i.e., $\overline{\mu_{\mathrm{G}}}^{*} = 0$, $\mu^{*}_{\mathrm{L}} = 0$, and $C_D \neq 0$), and thermal and viscous effects (i.e., $\overline{\mu_{\mathrm{G}}}^{*} \neq 0$, $\mu^{*}_{\mathrm{L}} \neq 0$, and $C_D = 0$), respectively.

The black dashed curve is almost uniform in the range of the practical wavenumber, indicating that small perturbations in the initial state are maintained in the time lapse. However, the blue and orange curves slightly and remarkably exceeded the unity, suggesting that small perturbations of high wavenumbers grow in the time lapse. On the other hand, the green curve became under the unity. This figure indicates that the energy conservation and the drag force lead to the instability of the two-fluid model equations, and the bulk viscosity make the model stable. Regarding the former, this result was opposite from that reported in Pokharna et al. (1997), which showed that the strong instability of the two-fluid model equations without bubble oscillations could be improved by considering the drag. Regarding the latter,

this result followed the same trend as that reported in Arai (1980), which showed that the bulk viscosity improved the ill-posed two-fluid model equations without bubble oscillations. The purple curve in Fig. 5 (a), which is proposed model, showed that considering both the bulk viscosity and drag caused strong dissipations. Our results suggested that the two-fluid model equations with bubble oscillations can be strongly stabilized by incorporating both the bulk viscosity and drag force.

4. Conclusions

We derived the averaged two-fluid model equations with bubble oscillations by incorporating the viscous and thermal effects into the original two-fluid model proposed by Egashira et al. (2004), which can describe the cavitating bubbly flow and pressure wave propagation in the bubbly flow. The highlights of the derivation can be summarised as follows:
(i) The volume-averaging process was used to evaluate the bubble oscillation behavior.
(ii) The viscous effect, which contains the bulk viscosity and drag, was incorporated into momentum conservations in the gas and liquid. The bulk viscosity led to the incorporation of additional terms (11) into the volume-averaged conservations. The drag was introduced by transforming the interfacial shear stress term (23).
(iii) The energy conservation for two-phase flows was derived with the thermal conduction in gas bubbles and the heat transfer between the two phases (37). The interfacial temperature gradient term for the thermal conduction was closed using the constitutive equations for a single bubble to limit the energy conservation to that for the bubbly flow. The alternative methods proposed to close the temperature gradient term for the thermal conduction were the differential equation for the gas pressure (41) and the temperature gradient models (42).

The stability analysis was conducted to investigate the dynamic character of our proposed two-fluid model equations with bubble oscillations, and the linear dispersion analysis was used to evaluate the behavior of small perturbations from a steady state of the model equations. The main results are summarized as follows:
(iv) Closing the temperature gradient term for the thermal conduction using the differential equation for the gas pressure resulted in an extremely large amplification factor, which then could cause a divergence of the solutions.

By contrast, closing the temperature gradient term using the temperature gradient models stabilized our proposed model. Therefore, we conclude that the temperature gradient models should be used to close the energy conservation (51).
(v) The linear dispersion analysis revealed that the thermal conduction inside bubbles was dominant in the thermal damping of bubble oscillations in bubbly flows rather than the heat transfer between the two phases.
(vi) The two-fluid model equations with bubble oscillations were unstable for considering the thermal effect and the drag; however were strongly stabilized, which considered both the bulk viscosity and the drag. This result indicates that the incorporation of the bulk viscosity and the drag plays an important role in stabilizing our proposed model.

Our results was important for developing mathematical models to investigate thermal effects in bubbly flow with bubble oscillations, such as cavitating bubbly flow and wave propagation in bubbly liquids. Verifying the numerical stability of our proposed model equations in the 2D or 3D is very important (Vaidheeswaran and Lopez de Bertodano, 2017; Panicker et al., 2018) and will be conducted in a forthcoming paper.

Acknowledgement

This work was partially funded by the JSPS KAKENHI (T.A., Grant number 21J20389), (T.K., Grant numbers 18K03942, 22K03898); the New Energy and Industrial Technology Development Organisation (Grant number JPNP20004); the Komiya Research Grant from the Turbomachinery Society of Japan; and the JKA promotion funds from KEIRIN RACE.

Appendix A. Coefficients of linearised presented two-fluid model equations

The matrixes $\mathbf{A}^*, \mathbf{B}^*, \mathbf{C}^*, \mathbf{D}^*$ in Eq. (60) are defined as,

$$\mathbf{A}^* = \begin{bmatrix} A_{11} & 0 & 0 & 0 & 0 & A_{16} & 0 \\ A_{21} & 0 & 0 & A_{24} & 0 & 0 & 0 \\ A_{31} & A_{32} & A_{33} & A_{34} & 0 & A_{36} & 0 \\ A_{41} & A_{42} & A_{43} & A_{44} & 0 & 0 & 0 \\ 0 & 0 & 0 & 0 & A_{55} & 0 & 0 \\ 0 & 0 & 0 & 0 & A_{65} & 0 & A_{67} \\ 0 & 0 & 0 & 0 & 0 & A_{76} & 0 \end{bmatrix}, \tag{A.1}$$

$$\mathbf{B}^* = \begin{bmatrix} B_{11} & B_{12} & 0 & 0 & 0 & B_{16} & 0 \\ B_{21} & 0 & B_{23} & B_{24} & 0 & 0 & \\ B_{31} & B_{32} & B_{33} & B_{34} & B_{35} & B_{36} & 0 \\ B_{41} & B_{42} & B_{43} & B_{44} & 0 & 0 & 0 \\ 0 & B_{52} & 0 & 0 & B_{55} & 0 & 0 \\ 0 & 0 & 0 & 0 & 0 & 0 & 0 \\ 0 & 0 & 0 & 0 & 0 & 0 & 0 \end{bmatrix}, \tag{A.2}$$

$$\mathbf{C}^* = \begin{bmatrix} 0 & 0 & 0 & 0 & 0 & 0 & 0 \\ 0 & 0 & 0 & 0 & 0 & 0 & 0 \\ C_{31} & C_{32} & 0 & 0 & 0 & C_{36} & 0 \\ C_{41} & 0 & C_{43} & 0 & 0 & C_{46} & 0 \\ C_{51} & 0 & 0 & 0 & C_{55} & 0 & 0 \\ 0 & 0 & 0 & 0 & 0 & 0 & 0 \\ 0 & 0 & 0 & 0 & 0 & 0 & 0 \end{bmatrix}, \tag{A.3}$$

and

$$\mathbf{D}^* = \begin{bmatrix} 0 & 0 & 0 & 0 & 0 & 0 & 0 \\ 0 & 0 & 0 & 0 & 0 & 0 & 0 \\ D_{31} & D_{32} & D_{33} & D_{34} & 0 & D_{36} & 0 \\ D_{41} & D_{42} & D_{43} & D_{44} & 0 & D_{46} & 0 \\ D_{51} & 0 & 0 & 0 & D_{55} & D_{56} & 0 \\ 0 & 0 & 0 & D_{64} & D_{65} & D_{66} & D_{67} \\ 0 & 0 & 0 & 0 & 0 & 0 & D_{77} \end{bmatrix}, \tag{A.4}$$

The elements of the above coefficient matrixes are given as,

$$
\begin{aligned}
&A_{11}=1,\quad A_{16}=-3,\quad A_{21}=-\alpha_0^*,\quad A_{24}=(1-\alpha_0^*)\frac{p_{\mathrm{L0}}^*}{{c_{\mathrm{L0}}^*}^2},\\
&A_{31}=\rho_{\mathrm{G0}}^* u_{\mathrm{G0}}^*+\beta_2^*(u_{\mathrm{G0}}^*-u_{\mathrm{L0}}^*),\quad A_{32}=\rho_{\mathrm{G0}}^*+\beta_1^*,\quad A_{33}=-\beta_1^*,\\
&A_{34}=\beta_3^*(u_{\mathrm{G0}}^*-u_{\mathrm{L0}}^*)\frac{p_{\mathrm{L0}}^*}{{c_{\mathrm{L0}}^*}^2},\quad A_{36}=-3\rho_{\mathrm{G0}}^* u_{\mathrm{G0}}^*,\\
&A_{41}=-\alpha_0^*[u_{\mathrm{L0}}^*+\beta_2^* u_{\mathrm{G0}}^*(u_{\mathrm{G0}}^*-u_{\mathrm{L0}}^*)],\quad A_{42}=-\beta_1^*\alpha_0^*,\\
&A_{43}=1-\alpha_0^*+\beta_1^*\alpha_0^*,\quad A_{44}=[(1-\alpha_0^*)u_{\mathrm{L0}}^*-\beta_3^*\alpha_0^*(u_{\mathrm{G0}}^*-u_{\mathrm{L0}}^*)]\frac{p_{\mathrm{L0}}^*}{{c_{\mathrm{L0}}^*}^2},\\
&A_{65}=-\frac{p_{\mathrm{G0}}^*}{\Delta^* c_{\mathrm{L0}}^*},\quad A_{67}=1+\frac{4\mu_{\mathrm{L}}^*}{\Delta^* c_{\mathrm{L0}}^*},\quad A_{76}=1,
\end{aligned}
\tag{A.5}
$$

$$
\begin{aligned}
&B_{11}=u_{\mathrm{G0}}^*,\quad B_{12}=1,\quad B_{16}=-3u_{\mathrm{G0}}^*,\quad B_{21}=-\alpha_0^* u_{\mathrm{L0}}^*,\quad B_{23}=1-\alpha_0^*,\\
&B_{24}=(1-\alpha_0^*)\frac{u_{\mathrm{L0}}^* p_{\mathrm{L0}}^*}{c_{\mathrm{L0}}^2},\quad B_{31}=[\rho_{\mathrm{G0}}^* u_{\mathrm{G0}}^*+\beta_2^*(u_{\mathrm{G0}}^*-u_{\mathrm{L0}}^*)]u_{\mathrm{G0}},\\
&B_{32}=(2\rho_{\mathrm{G0}}^*+\beta_1^*)u_{\mathrm{G0}}^*,\quad B_{33}=-\beta_1^* u_{\mathrm{L0}}^*,\quad B_{34}=\beta_3^* u_{\mathrm{G0}}^*(u_{\mathrm{G0}}^*-u_{\mathrm{L0}}^*)\frac{p_{\mathrm{L0}}^*}{c_{\mathrm{L0}}^2},\\
&B_{35}=p_{\mathrm{G0}}^*,\quad B_{36}=-3(p_{\mathrm{G0}}^*+\rho_{\mathrm{G0}}^* u_{\mathrm{G0}}^2),\\
&B_{41}=-\alpha_0^*\big[u_{\mathrm{L0}}^2+\beta_2^* u_{\mathrm{G0}}^*(u_{\mathrm{G0}}^*-u_{\mathrm{L0}}^*)\big],\quad B_{42}=-\beta_1^*\alpha_0^* u_{\mathrm{G0}}^*,\\
&B_{43}=[2(1-\alpha_0^*)+\beta_1^*\alpha_0^*]u_{\mathrm{L0}},\\
&B_{44}=1-\alpha_0^*+\big[(1-\alpha_0^*)u_{\mathrm{L0}}^2-\beta_3^*\alpha_0^*(u_{\mathrm{G0}}^*-u_{\mathrm{L0}}^*)\big]\frac{p_{\mathrm{L0}}^*}{c_{\mathrm{L0}}^2},\quad B_{52}=\alpha_0^* p_{\mathrm{G0}}^*,\\
&B_{56}=\alpha_0^* c_{\mathrm{V}}^* \rho_{\mathrm{G0}}^* u_{\mathrm{G0}}^*,
\end{aligned}
\tag{A.6}
$$

$$
C_{32}=-\mu_{\mathrm{G0}}^*,\quad C_{43}=-(1-\alpha_0^*)\mu_{\mathrm{L}}^*,\quad C_{51}=-\alpha_0^*\Delta^2(\lambda_{\mathrm{G}}^*-\lambda_{\mathrm{L}}^*),\quad C_{55}=-\alpha_0^*\Delta^2\lambda_{\mathrm{G}}^*,
\tag{A.7}
$$

and

$$D_{31}=\pm\frac{3}{8}\frac{C_D^*}{\Delta^*}(u_{\mathrm{G0}}^*-u_{\mathrm{L0}}^*)^2,\quad D_{32}=\pm\frac{3}{4}\frac{C_D^*}{\Delta^*}(u_{\mathrm{G0}}^*-u_{\mathrm{L0}}^*),$$
$$D_{33}=\mp\frac{3}{4}\frac{C_D^*}{\Delta^*}(u_{\mathrm{G0}}^*-u_{\mathrm{L0}}^*),\quad D_{34}=\pm\frac{3}{8}\frac{C_D^*}{\Delta^*}(u_{\mathrm{G0}}^*-u_{\mathrm{L0}}^*)^2\frac{p_{\mathrm{L0}}}{c_{\mathrm{L0}}^2},$$
$$D_{36}=\mp\frac{3}{8}\frac{C_D^*}{\Delta^*}(u_{\mathrm{G0}}^*-u_{\mathrm{L0}}^*)^2,\quad D_{41}=\mp\frac{3\alpha_0^*}{8}\frac{C_D^*}{\Delta^*}(u_{\mathrm{G0}}^*-u_{\mathrm{L0}}^*)^2,$$
$$D_{42}=\mp\frac{3\alpha_0^*}{4}\frac{C_D^*}{\Delta^*}(u_{\mathrm{G0}}^*-u_{\mathrm{L0}}^*),\quad D_{43}=\pm\frac{3\alpha_0^*}{4}\frac{C_D^*}{\Delta^*}(u_{\mathrm{G0}}^*-u_{\mathrm{L0}}^*),$$
$$D_{44}=\mp\frac{3\alpha_0^*}{8}\frac{C_D^*}{\Delta^*}(u_{\mathrm{G0}}^*-u_{\mathrm{L0}}^*)^2\frac{p_{\mathrm{L0}}^*}{c_{\mathrm{L0}}^2},\quad D_{46}=\pm\frac{3\alpha_0^*}{8}\frac{C_D^*}{\Delta^*}(u_{\mathrm{G0}}^*-u_{\mathrm{L0}}^*)^2,$$
$$D_{64}=\frac{p_{\mathrm{L0}}^*}{\Delta^2},\quad D_{65}=-\frac{p_{\mathrm{G0}}^*}{\Delta^2},\quad D_{66}=\frac{3p_{\mathrm{G0}}^*-2\sigma^*}{\Delta^2},$$
$$D_{67}=\frac{3p_{\mathrm{G0}}^*-2\sigma^*}{\Delta^* c_{\mathrm{L0}}^*}+\frac{4\mu_{\mathrm{L}}^*}{\Delta^2},\quad D_{77}=-1, \tag{A.8}$$

where the operators $\pm$ and $\mp$ become $+$ and $-$ for $u_{\mathrm{G0}}\geq u_{\mathrm{L0}}$ and $u_{\mathrm{G0}}<u_{\mathrm{L0}}$, respectively.

Especially, the elements for case 1 are given as,

$$C_{31}=0,\quad C_{36}=0,\quad C_{41}=0,\quad C_{46}=0, \tag{A.9}$$

these for case 2 are given as,

$$C_{31}=-\alpha_0^*\mu_{\mathrm{G0}}^*u_{\mathrm{G0}}^*,\quad C_{36}=0,\quad C_{41}=\alpha_0^*(1-\alpha_0^*)\mu_{\mathrm{L}}^*u_{\mathrm{L0}}^*,\quad C_{46}=0, \tag{A.10}$$

these for case 1 are given as,

$$C_{31}=0,\quad C_{36}=3\alpha_0^*\mu_{\mathrm{G0}}^*u_{\mathrm{G0}}^*,\quad C_{41}=0,\quad C_{46}=-(1-\alpha_0^*)\mu_{\mathrm{L}}^*u_{\mathrm{L0}}^*\frac{p_{\mathrm{L0}}^*}{c_{\mathrm{L0}}^2}, \tag{A.11}$$

these for case A are given as,

$$A_{55}=\alpha_0^*c_{\mathrm{V}}^*\rho_{\mathrm{G0}}^*-\frac{\alpha_0^*p_{\mathrm{G0}}^*}{\kappa^*-1},\quad A_{56}=-3\alpha_0^*p_{\mathrm{G0}}^*,\quad D_{51}=0,\quad D_{55}=0,\quad D_{56}=0, \tag{A.12}$$

and these for case B are given as,

$$A_{55}=\alpha_0^*c_{\mathrm{V}}^*\rho_{\mathrm{G0}}^*-3\alpha_0^*\lambda_{\mathrm{G}}^*\frac{R_0\,\mathrm{Im}(\widetilde{L}_p)}{T\omega_{\mathrm{B}}|\widetilde{L}_p|^2},\quad A_{56}=0,\quad D_{51}=-3\alpha_0^*\lambda_{\mathrm{G}}^*\Lambda_1^*(T_{\mathrm{L}}^*-1),$$
$$D_{55}=3\alpha_0^*\lambda_{\mathrm{G}}^*\Lambda_1^*,\quad D_{56}=3\alpha_0^*\lambda_{\mathrm{G}}^*\Lambda_1^*(T_{\mathrm{L}}^*-1)^*, \tag{A.13}$$

where

$$\Lambda_1 = \begin{cases} \dfrac{R_0}{\sqrt{2\pi D/\omega_{\mathrm{B}}}} & : \text{LSM model} \\ \dfrac{R_0}{|\widetilde{L}_p|^2} & : \text{PCB model} \\ \dfrac{R_0\,\mathrm{Re}(\widetilde{L}_p)}{|\widetilde{L}_p|^2} & : \text{STM model} \end{cases} \tag{A.14}$$

References

Antal, S., Lahey, R., Flaherty, J., 1991. Analysis of phase distribution in fully developed laminar bubbly two-phase flow. Int. J. Multiph. Flow 17, 635–652.

Arai, M., 1980. Characteristics and stability analyses for two-phase flow equation systems with viscous terms. Nucl. Sci. Eng. 74, 77–83.

de Bertodano, M.L., Fullmer, W., Clausse, A., 2016. One-dimensional two-fluid model for wavy flow beyond the kelvin-helmholtz instability: Limit cycles and chaos. Nucl. Eng. Des. 310, 656–663.

Brennen, C., 2005. Fundamentals of Multiphase Flows. Cambridge University Press.

Caflisch, R., Miksis, M., Papanicolaou, G., Ting, L., 1985. Effective equaitons for wave propagaiton in bubbly liquids. J. Fluid Mech. 153, 259–273.

Carrillo, F., Bourg, I., Soulaine, C., 2020. Multiphase flow modeling in multiscale porous media: An open-source micro-continuum approach. J. Comput. Phys. 8, 100073.

Chuang, T., Hibiki, T., 2017. Interfacial forces in two-phase numerical simulation. Int. J. Heat Mass Transf. 113, 741–754.

Clausse, A., Chetty, K., Buchanan, J., Ram, R., de Bertodano, M.L., 2022. Kinematic stability and simulations of the variational two-fluid model for slug flow. Phys. Fluids 34, 043301.

van Deemter, J., van der Laan, E., 1961. Momentum and energy balances for dispersed two-phase flow. Appl. Sci. Res. 10, 102–108.

Deuben, B., Wang, Y., Oberlack, M., 2022. A deterministic two-phase model for an active suspension with non-spherical active particles using the eulerian spatial averaging theory. Phys. Fluids 34, 023302.

Drew, D., 1983. Mathematical modeling of two-phase flow. Annu. Rev. Fluid Mech. 15, 261–291.

Drew, D., Cheng, L., Lahey, R., 1979. The analysis of virtual mass effects in two-phase flow. Int. J. Multiph. Flow 5, 233–242.

Drew, D., Passman, S., 1998. Theory of multicomponent fluids. Springer Verlag, New York.

Eames, I., Hunt, J., 2004. Forces on bodies moving unsteadily in rapidly compressed flows. J. Fluid Mech. 505, 349–364.

Egashira, R., Yano, T., Fujikawa, S., 2004. Linear wave propagation of fast and slow modes in mixtures of liquid and gas bubbles. Flu. Dyn. Res. 34.

Fox, R., Laurent, F., Vié, A., 2020. A hyperbolic two-fluid model for compressible flows with arbitrary material-density ratios. J. Fluid Mech. 903, A5.

Fuster, D., Montel, F., 2015. Mass transfer effects on linear wave propagation in diluted bubbly liquids. J. Fluid Mech. 779, 598–621.

Habiyaremye, V., Komen, E., Kuerten, J., Frederix, E., 2022. Modeling of bubble coalescence and break-up using the log-normal method of moments. Chem. Eng. Sci. 253, 117577.

Ishii, M., 1975. Thermo-fluid dynamic theory oftwo-phase flow. Paris: Eyrolles.

Ishii, M., Hibiki, T., 2010. Thermo-Fluid Dynamics of Two-Phase Flow. Springer Science & Business Media.

Ishii, M., Mishima, K., 1980. Study of two-fluid model and interfacial area. Argonne National Lab, IL (USA) .

Ishii, M., Zuber, N., 1979. Drag coefficient and relative velocity in bubbly droplet or particulate flows. AIChE J. 25, 843–855.

Joseph, D., Lundgren, T., Jackson, R., Saville, D.A., 1990. Ensemble averaged and mix- ture theory equations for incompressible fluid-particle suspensions. Int. J. Multiph. Flow 16, 35–42.

Kameda, M., Matsumoto, Y., 1996. Shock waves in a liquid containing small gas bubbles. Phys. Fluids 8, 322–335.

Kamei, T., Kanagawa, T., Ayukai, T., 2021. An exhaustive theoretical analysis of thermal effect inside bubble for weakly nonlinear pressure waves in bubbly liquids. Phys. Fluids 33, 053302.

Kanagawa, T., Yano, T., Watanabe, M., Fujikawa, S., 2010. Unified theory based on parameter scaling for derivation of nonlinear wave equations in bubbly liquids. Journal of Fluid Science and Technology 3, 351–369.

Kataoka, I., 2001. Basic and constitutive equations based on modeling of gas-liquid two-phase flow. Japanese J. Multiphase Flow 15, 4–13.

Keller, J., Kolodner, I., 1956. Damping of nuderwater explosion bubble oscillations. J. Appl. Phys. 27, 1152–1161.

Lahey, R., Cheng, L., Drew, D., Flaherty, J., 1980. The effect of virtual mass on the numerical stability of accelerating two-phase flows. Int. J. Multiphase Flow 6, 281–294.

Lee, S., Lee, J., Kim, B., 2017. Improvement of the two-fluid momentum equaiton using a modified reynolds sterss model for horizontal turbulent bubbly flows. Chem. Eng. Sci. 173, 208–217.

Lertnuwat, B., Sugiyama, K., Matsumoto, Y., 2001. Modelling of thermal behavior inside a bubble. Proceedings of 4th International Symposium on Cavitation , B6.002.

Levich, L., 1962. Physicochemical hydrodynamics. Englewood Cliffs, NJ: Prentice-Hall.

Lhuillier, D., Chang, C., Theofanous, T., 2013. On the quest for a hyperbolic effective-field model of disperse flow. J. Fluid Mech. 731, 184–194.

Lubchenko, N., Magolan, B., Sugrue, R., Baglietto, E., 2018. A more fundamental wall lubrication force from turbulent dispersion regularization for multiphase cfd applications. Int. J. Multiph. Flow 98, 36–44.

Lyczkowski, R., Gidaspow, D., Solbrig, C., Hughes, E., 1978. Characteristics and stability analyses of transient one-dimensional two-phase flow equations and their finite difference approximations. Nucl. Sci. Eng. 66.

Nagrani, P., Municchi, F., Marconnet, A., Christov, I., 2022. Two-fluid modeling of heat transfer in flows of dense suspensions. Int. J. Heat Mass Transfer 183, 122068.

Nigmatulin, R., 1979. Spatial averaging in the mechanics of heterogeneous and dispersed systems. Int. J. Multiph. Flow 5, 353–385.

Nigmatulin, R., Khabeev, N., Nagiev, F., 1981. Dynamics, heat, and mass transfer in vapor-gas bubbles in a liquid. Int. J. Heat Mass Transfer 24, 1033–1044.

Pal, R., K, R., 2021. Thermo-hydrodynamic modeling of flow boiling through the horizontal tube using eulerian two-fluid modeling approach. Int. J. Heat Mass Transfer 168, 120794.

Panicker, N., Passalacqua, A., Fox, R., 2018. On the hyperbolicity of the two-fluid model for gas-liquid bubbly flows. Appl. Math. Model. 57.

Park, J., Drew, D., Lahey, R., 1998. The analysis of void wave propagation in adiabatic monodispersed bubbly two-phase flows using an ensemble averaged two-fluid model. Int. J. Multiphase Flow 24, 1205–1244.

Pauchon, C., Banerjee, S., 1986. Interphase momentum interaction effects in the averaged multifield model, part1: void propagation in bubbly flows. Int. J. Multiphase Flow 12, 559–573.

Pokharna, H., Mori, M., Ransom, V., 1997. Regularization of two-phase flow models: A comparison of numerical and differential approaches. J. Comput. Phys. 134, 282–295.

Preston, A., Colonius, T., Brennen, C.E., 2002. A reduced-order model of heat transfer effects on the dynamics of bubbles. Proceedings of ASME FEDSM ' 02 , FEDSM2002–31026(CD–ROM).

Prosperetti, A., 1991. The thermal behavior of oscillating gas bubbles. J. Fluid Mech. 222, 587–616.

Prosperetti, A., Crum, L., Commander, K., 1988. Nonlinear bubble dynamics. J. Acoust. Soc. Am. 83, 502–514.

Prosperetti, A., Jones, A., 1984. Pressure forces in disperse two-phase flow. Int. J. Multiphase Flow 10.

Prosperetti, A., Tryggvason, G., 2007. Computational Methods for Multiphase Flow. Cambridge Univ. Press, London.

Ramshaw, J., Trapp, J., 1978. Characteristics, stability, and short-wavelength phenomena in two-phase flow equations systems. Nucl. Sci. Eng. 66, 93–102.

Ransom, V., Hicks, D., 1984. Hyperbolic two-pressure models for two-phase flow. J. Comput. Phys. 53, 124–151.

Rayleigh, L., 1917. Viii. on the pressure developed in a liquid during the collapse of a spherical cavity. Phil. Mag. 34, 94–98.

Rezende, R., Almeida, R., de Souza, A.U., Souza, S.G.U., 2015. Atwo-fluid model with a tensor closure model approach for free surface flow simulations. Chem. Eng. Sci. 122, 596–613.

Sato, Y., Sekoguchi, K., 1975. Liquid velocity distribution in two-phase bubble flow. Int. J. Multiph. Flow 2, 79–95.

Schiller, L., Naumann, A., 1933. Über die grundlegenden berechnungen bei der schwerkraft- aufbereitung. Zeitschrift des Vereines Deutscher Ingenieure 77, 318–320.

Shi, S., Liu, Y., Yilgor, I., Sabharwall, P., 2022. A two-phase three-field modeling framework for heat pipe application in nuclear reactors. Ann. Nucl. Energy 165, 108770.

Slattery, J., 1967. Flow of viscoelastic fluids through porus media. AIChE J. 13.

Stuhmiller, J., 1977. The influence of interfacial pressure forces on the character of two-phase flow model equations. Int. J. Multiphase Flow 3, 551–560.

Sugiyama, K., Takagi, S., Matsumoto, Y., 2005a. A new reduced-order model for the thermal damping effect on radial motion of a bubble (1st report, perturbation analysis). Trans. JSME, Ser. B 71, 1011–1019.

Sugiyama, K., Takagi, S., Matsumoto, Y., 2005b. A new reduced-order model for the thermal damping effect on radial motion of a bubble (2st report, validation of the model by numerical simulation). Trans. JSME, Ser. B 71, 1239–1246.

Tanamachi, Y., Takahashi, R., 1995. Ill-posedness of two-fluid model and regularization by second-order spatial derivative term. Journal of the Atomic Energy Society of Japan 37.

Tomiyama, A., Kataoka, I., Zun, I., Sakaguchi, T., 1998. Drag coefficients of single bubbles under normal and micro gravity conditions. JSME Int. J. Series B 41, 472–479.

Tukhvatullina, R., Frolov, S., 2018. Well-posed euler model of shock-induced two-phase flow in bubbly liquid. Shock Waves 28, 253–266.

Vaidheeswaran, A., Lopez de Bertodano, M., 2016. Interfacial pressure coefficient for ellipsoids and its effect on the two-fluid model eigenvalues. J. Fluids Eng. 138, 081302.

Vaidheeswaran, A., Lopez de Bertodano, M., 2017. Stability and convergence of computational eulerian two-fluid model for a bubble plume. Chem. Eng. Sci. 160, 210–226.

Vaidheeswaran, A., Fullmer, W., Lopez de Bertodano, M., 2016. Effect of collision force on well-posedness and stability of the two-fluid model for vertical bubbly flows. Nucl. Sci. Eng. 184, 353–362.

Vaidheeswaran, A., Prabhudharwadkar, D., Guilbert, P., J.R. Buchanan, J., de Bertodano, M.L., 2017. New two-fluid model near-wall averaging and consistent matching for turbulent bubbly flows. J. Fluids Eng. 139, 011302.

Wallis, G., 1969. One-Dimensional Two-Phase Flow. McGraw Hill.

Warnez, M., Johnsen, E., 2015. Numerical modeling of bubble dynamics in viscoelastic media with relaxation. Phys. Fluids 27, 063103.

Whiaker, S., 1969. Advances in the theory of fluid motion in porus media. Ind. Eng. Chem. 61.

van Wijngaarden, L., 1968. On the equations of motion for mixtures of liquid and gas bubbles. J. Fluid Mech. 33, 465–474.

van Wijngaarden, L., 1972. One-dimensional flow of liquids containing small gas bubbles. Annual Review of Fluid Mechanics 4, 369–396.

Yabushita, Y., Tanamachi, Y., Shimoda, Y., Shimegi, N., 1995. Well-posedness for two-fluid two-phase flow equations. Journal of the Atomic Energy Society of Japan 37.

Yano, T., Egashira, R., Fujikawa, S., 2006. Linear analysis of dispersive waves in bubbly flows based on averaged equations. J. Phys. Soc. Jpn. 75, 104401.

Yatabe, T., Kanagawa, T., Ayukai, T., 2021. Theoretical elucidation of effect of drag force and translation of bubble on weakly nonlinear pressure waves in bubbly flows. Phys. Fluids 33, 033315.

Yilgor, I., Shi, S., 2022. Scaling laws for two-phase flow and heat transfer in high-temperature heat pipes. Int. J. Heat Mass Transfer 189, 122688.

Zhang, D., 2021. Ensemble average and nearest particle statistics in disperse multiphase flows. J. Fluid Mech. 910, A16.

Zhang, D., Prosperetti, A., 1994. Averaged equations for inviscid disperse two-phase flow. J. Fluid Mech. 267, 185–219.

Zuber, N., Findlay, J., 1965. Average volumetiric concentration in two-phase flow systems. J. Heat Transfer 87, 453–468.

Ẑun, I., 1980. The transverse migration of bubbles influenced by walls in vertical bubbly flow. Int. J. Multiph. Flow 6, 583–588.

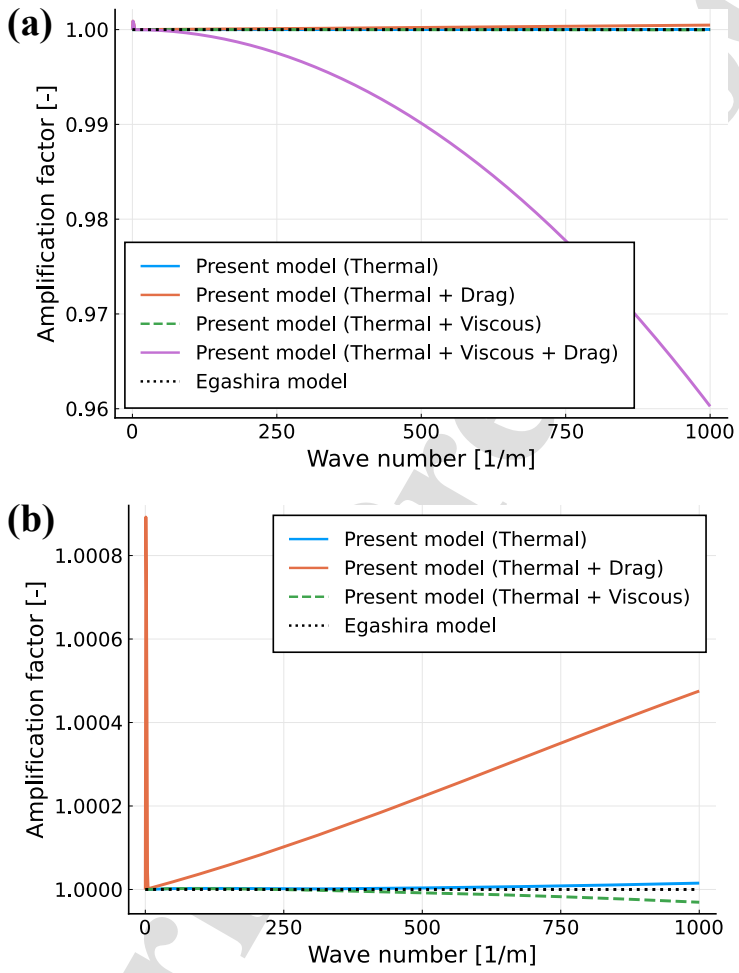

Figure 5: (a) Amplification factors versus the dimensional wavenumber. Purple, blue, orange, and green curves represent our proposed model, without the bulk viscosity and drag, without the bulk viscosity, and without the drag, respectively. The dashed black curve represents the two-fluid model proposed by Egashira et al. (2004), which corresponds to our proposed model without considering the bulk viscosity, drag, and energy conservation. The initial and physical parameters are the same as those in Fig. 2. (b) Enlarged view of (a) near unity of the amplification factor.

Two-fluid model with bubble oscillations was analytically derived by volume average

Interfacial term of energy conservation was closed by temperature gradient model

Stability analysis revealed that thermal conduction inside bubble was dominant

Viscosity and drag play an important role in stability of our derived two-fluid model

Declaration of interests

☒ The authors declare that they have no known competing financial interests or personal relationships that could have appeared to influence the work reported in this paper.

☐ The authors declare the following financial interests/personal relationships which may be considered as potential competing interests: